Annual Review of Heat Transfer, Volume 14, pp. 129-168 (2005)

CHAPTER

II.3

THERMAL CONDUCTION IN SILICON MICRO- AND NANOSTRUCTURES

A. D. McConnell and K. E. Goodson

Abstract

Silicon micro- and nanostructures are found in integrated circuits, sensors, and actuators, and the performance and reliability of many of these devices are affected by thermal conduction. Conduction processes in micro- and nanostructures are complicated by phonon interactions with grain and material boundaries. Phonon confinement in nanostructures and highly nonequilibrium rates of phonon generation by electrons also influence heat conduction. This article reviews experimental and theoretical studies of the thermal conductivity of single-crystal and polycrystalline silicon films, with a focus on data relevant for modeling heat transport in modern devices. Data for single-crystal films indicate a room-temperature thermal conductivity reduction of up to 50% compared to bulk silicon due to phonon boundary scattering, while grain boundary scattering in polysilicon films results in even lower values. Simple analytical expressions for approximating the room-temperature thermal conductivity of silicon films are provided. Doping modifies heat conduction mainly due to impurity scattering, and thermal conductivity data for boron-, phosphorus-, and arsenic-doped silicon films demonstrate the extent of this effect. Hotspots smaller than the phonon mean free path cause intense localized heating in silicon and severe departure from equilibrium within the phonon system, which can substantially increase the effective thermal resistance for conduction. This review provides an overview of the nanoscale conduction effects that are becoming important for the design of silicon nanostructures.

1-56700-222-6/04/$35.00+$00.00

1 INTRODUCTION

Silicon micro- and nanostructures are a central part of modern integrated circuits, sensors, and actuators. A large number of these devices experience significant heat transfer, which influences performance and reliability. For example, continually increasing current densities and shrinking device dimensions in electronic circuits [1] can lead to higher temperature differences within the silicon microprocessors. Since temperature governs the mean time to failure and channel mobility in silicon-based integrated circuits, performance optimization should include thermal effects [2]. This is especially critical in ultra-thin-body silicon-on-insulator (SOI) transistors that comprise a very thin single-crystal silicon device layer on top of a buried oxide layer. The low thermal conductivity of the oxide and the reduced thermal conductivity of the thin silicon layer, compared to the bulk, impede the conduction of heat generated during device operation away from the active regions [3]. Integrated circuits also commonly involve polycrystalline silicon films, with applications including the gate electrode in MOS devices, the intermediate conductor in two-level structures, thin-film high-value resistors, and ohmic contacts to shallow junctions [4]. Heat transfer affects MEMS devices containing silicon films, such as silicon AFM cantilevers that thermally read and write data in thin polymer films [5] and doped polysilicon resistive temperature sensors [6]. Modeling heat transport in integrated circuit and MEMS components requires accurate thermal conductivity values for silicon films.

There has been much research on thermal conduction in silicon. Experimental data for bulk silicon [7, 8] show that the sample size and purity affect thermal conductivity at low temperatures and that doping reduces the thermal conductivity due to impurity scattering. Based on the work of Klemens [9] and Callaway [10], Holland [11] developed a detailed thermal conductivity model specifically for silicon based on the phonon Boltzmann transport equation including semiempirical scattering rates to fit bulk data.

However, conduction processes in modern nanostructures can be substantially different from those in bulk samples, rendering the use of thermal conductivity values for bulk silicon inappropriate in most circumstances. While thermal conductivity is an intrinsic property of bulk materials at room temperature, the thermal conductivity of thin films depends on the film thickness and microstructure, due to the scattering of phonons (the dominant energy carriers in silicon) on film and grain boundaries which limits the phonon mean free path. Studies of silicon films have found that phonon boundary scattering reduces the room-temperature thermal conductivity by more than 10% compared to bulk silicon for films thinner than approximately 1 μm [12] and by up to 50% for films on the order of 100 nm [13]. This size effect becomes more pronounced at lower temperatures as the bulk mean free path increases. Dopant atoms reduce the thermal conductivity of silicon films [14, 15], and grain boundary scattering also significantly decreases room-temperature thermal conductivity values in polysilicon films [16–18]. For very thin silicon films and nanostructures, thermal conductivity models indicate that quantum effects, such as phonon confinement, influence heat conduction by altering phonon spectra [19].

Heat sources in silicon nanostructures smaller than the phonon mean free path, referred to as hotspots, cause intense localized heating and nonequilibrium heat conduction effects. Low-temperature experimental data show that the temperature in the vicinity of a hotspot exceeds that predicted by diffusion theory [20], which has important implications for the performance and operation of future silicon devices.

This article reviews experimental and theoretical studies of the thermal conductivity of single-crystal and polycrystalline silicon films and examines the differences between bulk and thin-film properties. Section 2 discusses thermal conductivity measurement methods, with a focus on those relevant to silicon films. Simulation techniques for modeling silicon thermal conductivity are summarized in Section 3, which also includes a brief discussion of the relevant fundamentals of phonon physics. Section 4 examines the size effect observed in the experimental data and provides simple, practical analytical expressions for predicting room-temperature thermal conductivity values. Doping effects in single-crystal silicon are presented in Section 5, and Section 6 reviews the impact of grain boundary scattering in polysilicon films. Section 7 focuses on localized hotspots in silicon nanostructures and their relevance to the operation of next-generation integrated circuits.

2 EXPERIMENTAL METHODS

This section briefly reviews experimental methods appropriate for measuring the in-plane and out-of-plane thermal conductivity components of thin silicon films, which yield data relevant for micro- and nanostructures. To obtain meaningful results, it is critical to understand the suitability and limitations of the various techniques, which depend on the film thickness, the expected thermal conductivity relative to that of the substrate or supporting measurement structure, and any sample preparation restrictions related to microstructural defects or device simulation requirements. Extensive reviews of experimental methods for thin-film thermal conductivity measurements are available [21–23], but this section focuses on electrical and optical techniques applicable to the study of silicon films.

Electrical experimental methods are based on passing current through a metal bridge machined on the sample film to generate Joule heat. This facilitates precise local heating, which tends to provide low experimental uncertainty relative to comparable laser heating techniques. Electrical-resistance thermometry, which uses the temperature-dependent change in resistivity of the heater material, determines temperature. Studies have used steady-state electrical techniques to measure the in-plane thermal conductivity of single-crystal silicon films [12, 14, 15, 24, 25] and polycrystalline silicon samples in the form of microcantilevers [16, 26–30], microbridges [31, 32], and suspended membranes [17, 18, 33, 34].

Figure 1 shows an example structure using DC heating and thermometry [14], in which a silicon film is suspended in a membrane fabricated with deep-etching processes. Current passed through the center aluminum bridge on top of the membrane creates a symmetric thermal gradient in the film, and two additional aluminum

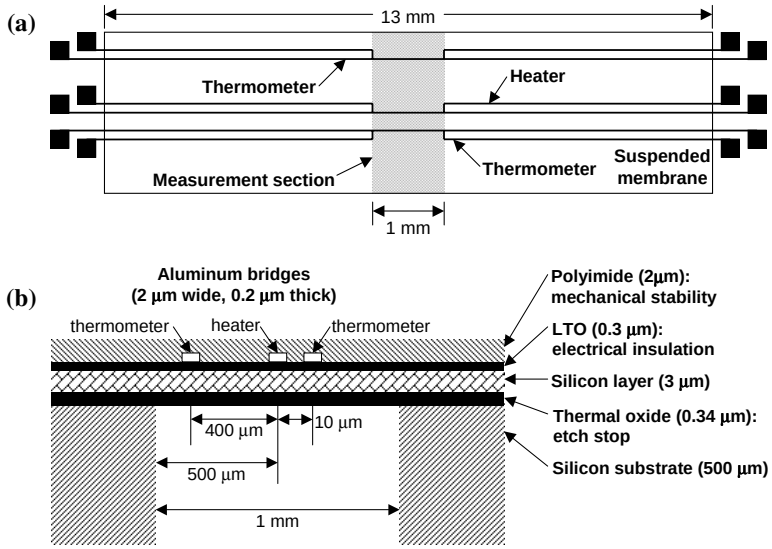

Figure 1 Schematic of an experimental structure for steady-state electrical in-plane thermal conductivity measurements [14]. The lateral and vertical dimensions are not in proportion: (a) top view and (b) side view.

lines serve as thermometers. The total length of the membrane is 13 mm, but the center 1 mm comprises the measurement region to avoid two-dimensional effects. The membrane is suspended to ensure that lateral conduction through the silicon film is the dominant heat transfer mode in the system. This simplifies data reduction and analysis by creating a one-dimensional heat conduction problem. Experimental instrumentation is straightforward, but the measurement structure requires a relatively involved fabrication process. This method is suitable for silicon samples with in-plane thermal conductivity values at least one order of magnitude larger than that of silicon dioxide, which is the passivation material between the sample and the metal heater lines.

The in-plane thermal conductivity of silicon films can also be measured using the 3ω method, a transient electrical technique developed by Cahill [35] to determine the out-of-plane thermal conductivity of disordered films, such as amorphous silicon dioxide, which has low thermal conductivity. For silicon, which has a substantially higher thermal conductivity, the 3ω method can actually be used to simultaneously determine the in-plane and out-of-plane components, since heat tends to spread within a silicon film. Such a measurement uses aluminum heater lines of varying widths patterned on top of a thermally isolated film [36, 37]. A heater line much wider than the film thickness independently determines the out-of-plane thermal conductivity, while narrower heater lines allow heat to spread both laterally and vertically through the film. Figure 2 illustrates the basic procedure with which Ju and Goodson [13] measured single-crystal silicon films using this technique. A si-

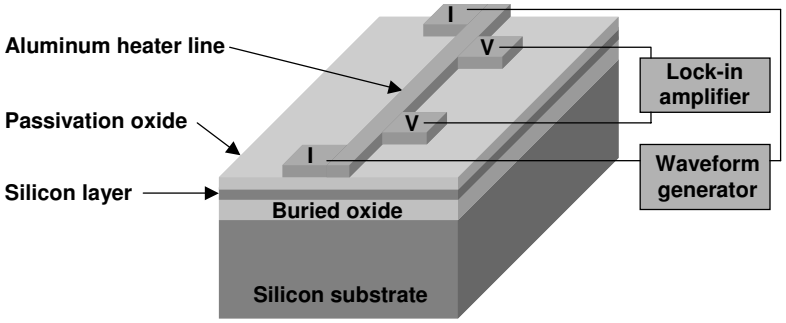

Figure 2 Schematic of an experimental structure for AC electrical in-plane and out-of-plane thermal conductivity measurements [13]. The dimensions are not in proportion.

nusoidally varying current at frequency ω produces Joule heating in the aluminum line at frequency 2ω, causing its temperature and resistance to also fluctuate at 2ω. This resistance fluctuation multiplied by the sinusoidal current results in a 3ω voltage component that can be detected with a lock-in amplifier. The temperature fluctuations consist of a frequency-dependent component due to substrate heating and a steady-state component from the film. A buried oxide layer ensures some lateral heat conduction in the silicon film due to the low oxide thermal conductivity. The solution to the two-dimensional heat conduction equation for the sample geometry yields the in-plane thermal conductivity component, given the independently-determined out-of-plane value as discussed above. While this technique requires a more complex data analysis compared to most steady-state methods, the measurement structure fabrication is less intricate. AC electrical methods are appropriate for the in-plane and out-of-plane thermal conductivity of silicon films or for the out-of-plane component of very thin films on a low thermal conductivity substrate, which limits the lateral spreading of heat within the film.

Compared to electrical measurement techniques, optical methods usually require less sample preparation, but data collection and analysis tend to be more complex. For example, while laser heating does not require sample contact, the exact amount of absorbed radiation is unknown. Separating the film properties from those of the underlying substrate is also a challenge in optical measurements, but pulsed laser heating at high frequencies can help [38]. One approach using optical methods for silicon film measurements is the thermal wave technique shown in Figure 3. This uses the interference of localized laser radiation with the sample surface to determine the lateral thermal conductivity of amorphous and polycrystalline silicon films on a fused quartz substrate [39]. The deflection of a probe beam detects the temporal decay of the spatially varying temperature field due to thermal expansion of the surface [21]. A substrate with low thermal diffusivity relative to the film ensures that most of the heat diffuses in the plane of the sample. The thermal properties of the film dominate the thermal waves in the air above the sample surface, which are probed near the heating spot using a He-Ne laser beam. Spatially-varying thermal

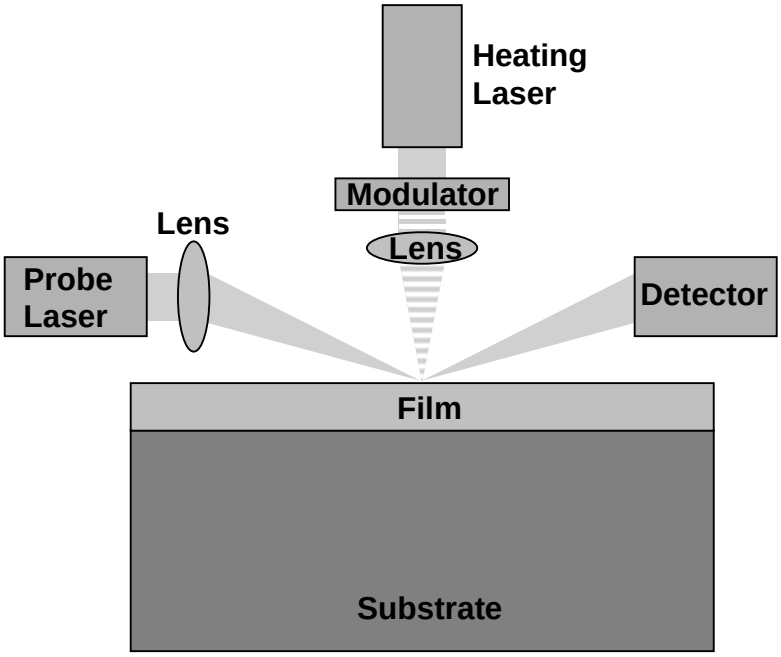

Figure 3 Side view of an experimental setup for the thermal wave technique to measure in-plane thermal conductivity [39].

wave profiles are fit to a solution of the three-dimensional heat diffusion equation for the system comprising the air, film, and substrate. This yields the lateral thermal diffusivity of the film, and the thermal conductivity is calculated from bulk silicon properties. This technique is appropriate for measuring the in-plane thermal conductivity of silicon films on low-thermal conductivity substrates.

3 SIMULATION TECHNIQUES

Simulations of thermal conduction in silicon films model phonon behavior, since phonons are the primary energy carriers. Phonons are the energy quanta of lattice vibrations and describe wave packets that can in most cases be modeled as particles. In silicon films, phonons can scatter on other phonons, electrons, impurities, defects, and film and grain boundaries, impeding heat conduction and lowering the thermal conductivity.

The first thermal conductivity models for bulk silicon [9–11] were based on solutions to the phonon Boltzmann transport equation using the relaxation time approximation and represented the various phonon scattering events with individual relaxation times. This formulation is appropriate for bulk silicon and for films with

thickness on the order of the phonon mean free path. However, as device dimensions shrink into the nanometer regime and begin to approach phonon wavelengths, models must include modifications to the phonon dispersion relation using either wave calculations or molecular dynamics. This section presents various simulation techniques appropriate for modeling thermal conductivity in silicon films, including the phonon Boltzmann transport equation, Monte-Carlo methods, the equation of phonon radiative transfer, and molecular dynamics. These techniques treat the basic phonon physics in silicon differently, and selection of a suitable method usually depends on the lengthscale of the system or effect being studied relative to the phonon mean free path.

3.1 Fundamentals of Heat Transport in Silicon

The plot of thermal conductivity k as a function of temperature T in Figure 4 illustrates the basic shape of this curve for bulk silicon and can be qualitatively interpreted using a simple thermal conductivity model from kinetic theory.

$$k = \frac{1}{3} C v_s \Lambda. \tag{1}$$

The average phonon group velocity v_s is assumed constant at a weighted average of the transverse and acoustic phonon velocities (6533 m/s) [11], while the phonon

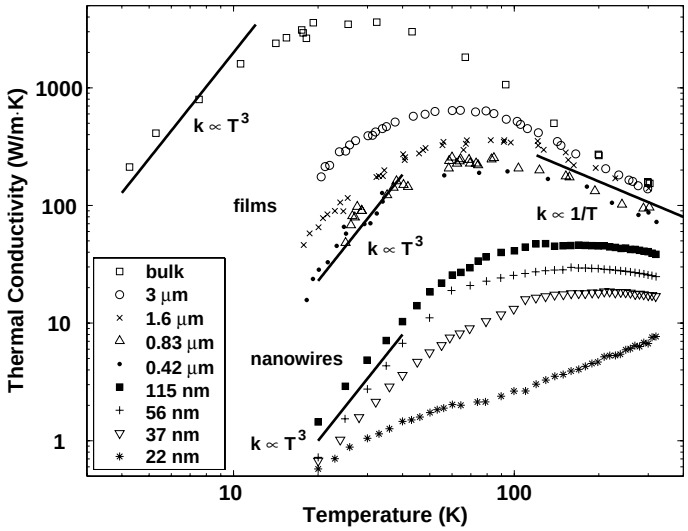

Figure 4 Thermal conductivity data as a function of temperature for single-crystal silicon demonstrating the size effect for thin films and nanowires and the T^3 and T^{-1} dependence at low and high temperatures, respectively, for a bulk sample. Experimental data come from the literature for bulk silicon [7], the 3 μm film [14], the 1.63, 0.83, and 0.42 μm films [12, 24], and the 115, 56, 37, and 22 nm nanowires [70].

mean free path Λ, effectively the average distance a phonon travels between scattering events, varies strongly with temperature. Using the Debye model (e.g., [40]), the specific heat C exhibits a cubic temperature dependence for low temperatures ($T < 0.1\theta_D$, $\theta_D = 645$ K in silicon) at which most phonons directly scatter on the film boundaries due to the low phonon population and the small number of intrinsic scattering events [41]. Assuming that the phonon mean free path equals the film thickness at low temperatures, the thermal conductivity is proportional to T^3. For temperatures above θ_D, the specific heat is constant and the dominant scattering mechanism is phonon-phonon Umklapp processes. Since the phonon population and collision frequency increase proportional to the temperature, the mean free path and thus the thermal conductivity both linearly decrease with increasing temperature, which represents the diffusive limit of phonon transport [41]. Between the low- and high-temperature regimes, the thermal conductivity reaches a peak that shifts to higher temperatures and lower values as impurity and defect concentrations increase. The various thermal conductivity modeling techniques presented in the following sections attempt to account for this behavior using different approximations of the phonon physics.

Although there are contributions to heat conduction in silicon from energy carriers other than phonons, including electrons, holes, and photons, these usually do not appreciably affect the thermal conductivity of silicon. At a given temperature, the electron contribution to the thermal conductivity k_e from free holes or electrons introduced by dopant atoms depends on the electrical resistivity ρ according to the Wiedemann-Franz law [40]. At room temperature the electrical resistivity of bulk silicon ranges between 10^{-4} and $2.3 \cdot 10^5$ Ωcm, corresponding to heavily doped (10^{21} cm^{-3}) and intrinsic silicon, respectively [42]. As an example, a value of $\rho = 4.5 \cdot 10^{-4}$ Ωcm [43] for bulk silicon doped with $3 \cdot 10^{20}$ cm^{-3} boron results in $k_e = 1.6$ W/m $\cdot$ K, which comprises only 3.4% of the total observed thermal conductivity of $k = 47$ W/m $\cdot$ K for this sample. The electronic contributions in lightly doped and intrinsic silicon are several orders of magnitude lower. However, above 1000 K in silicon, electron-hole pairs drifting down a temperature gradient carry a significant amount of energy. An analysis of bulk silicon data shows that at the melting point, phonons account for approximately 61% of the total thermal conductivity, electron-hole diffusion comprises 32%, free electrons or holes contribute 7%, and photons have a negligible effect [7].

3.2 The Boltzmann Transport Equation

Calculating the thermal conductivity of silicon requires a model that captures the phonon physics presented in the previous section. A suitable and widely-used formulation is the Boltzmann transport equation (BTE) for phonons, which is a statistical description of phonon behavior at a microscopic level.

The BTE uses a distribution function $f(\boldsymbol{r}, \boldsymbol{p}, t)$ to represent the number of phonons in a six-dimensional volume element of geometric space $\boldsymbol{r}$ and momentum space $\boldsymbol{p}$

as a function of time t:

$$\frac{\partial f}{\partial t} = -\boldsymbol{v}_g \cdot \nabla_r f - \boldsymbol{F} \cdot \nabla_p f + \left(\frac{\partial f}{\partial t}\right)_{\text{scat}}. \tag{2}$$

The left side of Eq. (2) is the total time rate of change of the distribution function, while the terms on the right correspond to diffusion in geometric space due to the phonon group velocity $\boldsymbol{v}_g$, acceleration in momentum space due to forces $\boldsymbol{F}$ imposed by external fields, and scattering due to all other processes, respectively [44].

Thermal conductivity relates a temperature gradient in a material to a heat flux,

$$\dot{\boldsymbol{q}}'' = k\nabla_r T, \tag{3}$$

which is the energy density of the system u multiplied by the phonon group velocity,

$$\dot{\boldsymbol{q}}'' = \boldsymbol{v}_g u = \sum_p \int_0^\infty \hbar\omega \, \boldsymbol{v}_g f D_p(\omega) d\omega, \tag{4}$$

where $\hbar\omega$ is the energy of one phonon. The sum is over all polarization modes P. The density of states for each mode $D_p(\omega)$ is integrated over all phonon frequencies ω to represent the quantized states that are available for phonon occupation, and the distribution function f from Eq. (2) describes how many phonons occupy these states. However, obtaining analytical solutions of Eq. (2) for even simple geometries is difficult since the scattering term is an integral over all wavevector states and the scattering rates depend on the number of particles, resulting in an integral-differential equation [44].

Solutions to Eq. (2) are possible using the relaxation time approximation [9, 10], which replaces the scattering term with the departure of the distribution function from equilibrium f_{de} divided by a relaxation time τ incorporating all phonon scattering events. For most thermal conductivity calculations, there are no external fields, the system is in steady state, and the departure of the system from equilibrium is small. Under these assumptions, Eq. (2) reduces to:

$$\frac{f_{\text{de}}}{\tau} = -\frac{\partial f_{\text{eq}}}{\partial T} \boldsymbol{v}_g \cdot \nabla_r T, \tag{5}$$

and f_{de} is substituted into Eq. (4) for f. For phonons, the equilibrium distribution function f_{eq} is the Bose – Einstein distribution:

$$f_{\text{eq}} = \frac{1}{\exp\left(\dfrac{\hbar\omega}{k_B T}\right) - 1}. \tag{6}$$

The relaxation time is the phonon mean free path divided by the average group velocity and represents the distance phonons travel between successive scattering

events. Matthiessen's rule calculates the overall scattering rate by summing individual scattering rates τ_j^{-1}, or inverse relaxation times, assuming that phonon scattering processes occur independently:

$$\tau^{-1} = \sum \tau_j^{-1}. \tag{7}$$

Empirical scattering rates for phonon-phonon interactions in bulk silicon are given by Holland [11], and Ziman [44] provides scattering rate equations for impurities, defects, and boundaries or interfaces.

Since the thermal conductivity of silicon depends on the phonon group velocity and density of states, phonon dispersion must be incorporated into thermal conductivity models. Phonon wave packets move with a group velocity defined as the derivative of angular frequency with respect to the wave vector. The slope of the phonon dispersion curves for silicon in Figure 5 gives the group velocity for each polarization branch and phonon type. Since silicon has two atoms per unit cell, there are both acoustic and optical phonons, each of which has one longitudinal and two transverse polarization branches. One common modeling approach is to neglect optical phonons due to their low group velocities and assume acoustic phonons are the main energy carriers. This is generally valid for thermal conductivity simulations. The De-

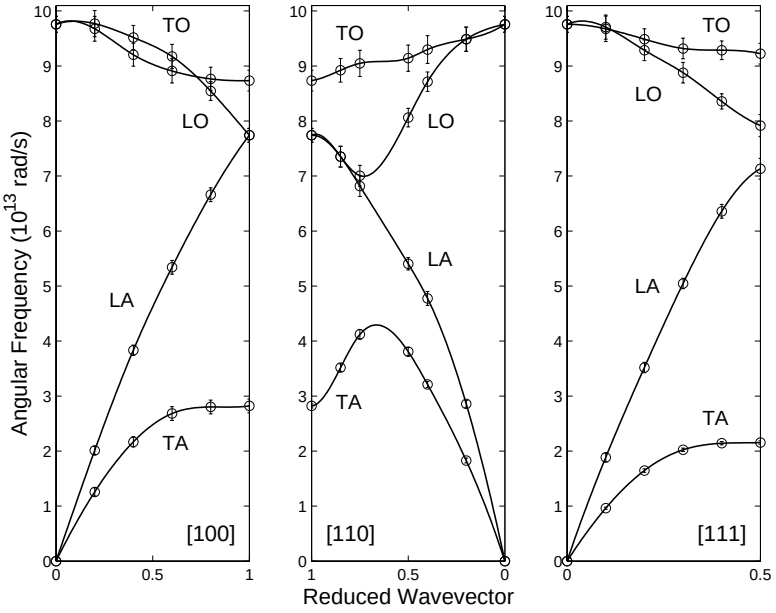

Figure 5 Phonon dispersion curves given as angular frequency ω versus reduced wave vector $K/K_{\max}$ for the [100], [110], and [111] directions in silicon based on neutron scattering data [99]. LA, TA, LO, and TO refer to the longitudinal acoustic, transverse acoustic, longitudinal optical, and transverse optical polarization branches, respectively. The two transverse phonon branches are degenerate in each of the directions shown in this figure.

bye model (e.g., [40]) also replaces the acoustic dispersion relations with a single average group velocity and assigns a cutoff frequency, which is the maximum allowed phonon frequency and thus the upper integration limit in Eq. (4). These approximations assume that the lattice vibrates as an elastic continuum, which is strictly valid only for low-frequency phonons whose wavelengths are much larger than the interatomic spacing. The silicon thermal conductivity model of Holland [11] provides an improved representation of phonon dispersion by assigning separate velocities to the low- and high-frequency portions of both the longitudinal and transverse acoustic branches. This approach was used to model the thermal conductivity of intrinsic and doped single-crystal silicon [12–14, 24] and polysilicon [17, 18] films. Under certain conditions, optical phonons may influence heat conduction in silicon (see Section 7) and can be represented using the Einstein approximation (e.g., [40]), which assumes all phonons vibrate at the same frequency. It is possible to include the entire phonon spectrum by calculating the dispersion relations from the equation of motion for an atom in an elastic continuum assuming isotropy [45], which is effective for studying phonon confinement in silicon [19].

3.3 Monte Carlo Methods

Monte Carlo methods are stochastic techniques already well-established for simulating electron behavior in semiconductor devices [46]. They provide a computationally efficient path to simulating complex behavior in large systems, so using Monte Carlo methods to solve the BTE requires fewer simplifying assumptions (such as those listed in the previous sections) compared to less sophisticated schemes.

Mazumder and Majumdar [47] developed a phonon Monte Carlo method based on the work of Peterson [48]. Their model allows phonons from the three directions in both geometric and wave-vector space to drift and scatter in time according to prescribed conditions based on the BTE and rules for phonon interactions. Unlike the Debye approximation, this model includes nonlinear phonon dispersion. The relaxation time approximation described in Section 3.2 is used to represent the various scattering processes, but they are considered independently instead of forming an overall relaxation time with Matthiessen's rule. Statistics sampled at various points in time and space under steady-state conditions determine thermal transport properties.

3.4 Phonon Physics in Silicon

Thermal conductivity models based on the BTE provide insight into which phonon polarization branch dominates heat transport. Phonon Monte Carlo simulations [47] of thermal conductivity data for intrinsic and 10^{19} cm^{-3} boron-doped silicon films 3 μm thick [14] show that at low temperatures most longitudinal acoustic (LA)

phonons leaving the hot side of the film reach the cold side. With increasing temperature, the average LA phonon lifetime decreases due to a large fraction transitioning to transverse acoustic (TA) phonons during three-phonon scattering processes, such that above 100 K the TA branch carries most of the energy. A BTE model of bulk silicon data also concludes that transverse phonons dominate heat conduction at high temperatures [11]. In contrast, a comparison of silicon thin-film data with a BTE solution has identified LA phonons as the main heat carriers at room temperature [13]. For other semiconductors such as germanium, gallium arsenide, and indium antimonide with phonon dispersion branches similar to silicon, various studies have found either LA or TA phonons as the main heat carriers (e.g., [49–51]). These disparate conclusions imply that simplifications made to the BTE could influence the results significantly. Most studies separately treat phonons from different branches and neglect transitions between branches [41], which is an overly simplistic approach but is usually necessary to solve the BTE. Both LA and TA phonons contribute to heat conduction in silicon due to their interaction during scattering events, although their relative contributions are expected to differ depending on temperature.

Within a given phonon branch, both low- and high-frequency phonons transport energy in silicon, but their relative contributions also depend on the temperature and on scattering events. For $T \ll \theta_D$, low-frequency phonons are the main heat carriers since higher frequencies are not populated [48]. At temperatures above θ_D, most phonons occupy states at the Debye cutoff frequency ω_D, so high-frequency phonon modes dominate thermal conduction due to their large number. However, lower-frequency phonons have longer mean free paths [52], and a BTE model of bulk silicon thermal conductivity shows that low-frequency phonons carry some heat at θ_D [11]. Various scattering events differently affect low-and high-frequency phonons. Point defects and impurities reduce thermal conductivity mainly at high frequencies since their scattering rates are proportional to ω^4 (see Section 5), while objects such as extended defects and grain boundaries with frequency-independent rates primarily scatter low-frequency phonons [52]. As an example, thermal conductivity data for silicon films irradiated with neutrons to produce substantial point-defect concentrations exhibits a much stronger size effect after irradiation [53]. Introducing point defects in silicon diminishes the contribution of high-frequency phonons, enhancing the relative effect of low-frequency phonon boundary scattering. Without low-frequency phonons, the sensitivity of thermal conductivity to point defects would be greater and the effects of extended defects and grain boundaries would be less prominent.

3.5 The Equation of Phonon Radiative Transfer

The equation of phonon radiative transfer (EPRT) treats phonon heat conduction as radiation during ballistic heat transport, in which the film thickness is much smaller than the phonon mean free path. This model assumes that phonons, as wave packets of energy, behave identically to photons by transforming the BTE in the relaxation

time approximation into a differential equation for phonon intensity, which then determines heat flux and thermal conductivity [41].

While extensive theory and analysis already exists for photon transport, it is not entirely appropriate to use expressions developed for photons to model phonons in silicon, since they do not account for nonlinear dispersion, the longitudinal polarization branch, and optical phonons. This approach assumes entirely diffuse boundary scattering, which is not necessarily true for ballistic transport processes [41]. Nevertheless, the EPRT has successfully predicted heat conduction in silicon crystals below 100 K, for which the mean free path is sufficiently long that heat conduction is in the ballistic regime [54]. Thermal conductivity models of silicon nanowires have used the EPRT [55, 56], but there is no experimental data to confirm these results. The ERPT works best for modeling ballistic heat conduction, which occurs in very thin silicon films at room temperature or in thicker films at low temperatures.

3.6 Molecular Dynamics

Molecular dynamics (MD) is an atomic-level simulation technique that solves equations of motion for atoms interacting with a prescribed energy potential. Thermal conductivity is calculated by applying a constant heat flux and setting appropriate boundary conditions.

For silicon, the Stillinger and Weber energy potential accurately predicts physical properties, such as the phonon dispersion curves [57]. The size of computational domain is critical, since the sample should be sufficiently small that code runs in a reasonable time but large enough to avoid finite-size effects [58]. MD thermal conductivity studies have successfully predicted values for bulk silicon [58–60] and silicon nanowires [61] and have demonstrated possible implementation strategies for modeling thin films [62–64] and porous silicon films [65]. MD simulations of phonon scattering at a semiconductor interface allow phonon transmission rates to be calculated as a function of frequency for the acoustic branches [66]. Incorporating detailed phonon transmission rates in a BTE or Monte Carlo thermal conductivity model could presumably improve the accuracy of these methods.

3.7 Summary

When modeling the thermal conductivity of silicon micro- and nanostructures, it is important to consider the relative merits and drawbacks of the various simulation approaches. Solutions to the phonon Boltzmann transport equation using the relaxation time approximation are suitable for bulk silicon and for structures with minimum dimensions as small as the phonon mean free path. Implementing the BTE can be relatively straightforward, but the separate treatment of scattering events using Matthiessen's rule oversimplifies actual phonon interactions. Using Monte Carlo methods to solve the BTE, it is possible to capture more detailed phonon physics such as non-linear dispersion, transitions between the different polarization branches, and

phonon creation and destruction due to scattering events. This formulation is also applicable for films of thickness on the order of the phonon mean free path but can be computationally expensive. For structures smaller than the phonon mean free path in which heat conduction is in the ballistic regime, the equation of phonon radiative transfer may be appropriate. While straightforward to implement, the EPRT does not incorporate nonlinear dispersion and assumes all boundary scattering is diffuse. As the size of silicon nanostructures approaches phonon wavelengths, atomic-level simulation techniques, such as molecular dynamics, are required. Molecular dynamics can more accurately represent physical parameters, such as phonon dispersion, and are currently feasible for studying very small systems, investigating specific nanoscale conduction phenomena, or modeling bulk samples to which periodic boundary conditions can be applied.

4 SIZE EFFECT IN FILMS AND NANOWIRES

The size effect in silicon refers to the thermal conductivity reduction observed for thin films compared to bulk silicon. The experimental thermal conductivity data for silicon films and nanowires shown in Figure 4 and Table 1 reveals qualitative information about the effects of film thickness (or nanowire diameter) and temperature on the thermal conductivity.

The thermal conductivity of samples $14.0-98.4\ \mu$m thick linearly decreases with the reciprocal of the square root of the thickness at 300 K and more noticeably at 200 K [67]. Measurements of films 4 μm [68], 3 μm [14], and 1.6 μm [24] thick show a room-temperature reduction smaller than the experimental error, while phonon-interface scattering reduces the room-temperature thermal conductivity of $74-240$ nm films up to 50% [13] and of a 0.42 μm film by 40% [24] compared to bulk silicon. A room-temperature value of less than 2.2 $\mathrm{W/m \cdot K}$, or approximately 1.5% of the bulk, for a 155 nm film [25] is inconsistent with data from all other experimental studies and may be due to high defect or dislocation densities caused by the fabrication and growth processes [69]. The thermal conductivity of a 115 nm diameter nanowire is reduced by a factor of nearly four compared to bulk silicon at room temperature, and smaller diameters result in lower values for all measured temperatures [70]. A significant thermal conductivity reduction is evident at temperatures below approximately 150 K for the 3 μm [14] and 1.6 μm [24] films, while the thermal conductivity of the 0.42 and 0.83 μm films is less than the bulk value for all temperatures below 300 K [24]. The data in Table 1 indicates a significant size effect at room temperature for films less than approximately 1 μm thick, and Figure 4 clearly shows that the size effect is most prominent for low temperatures, at which the phonon mean free path in bulk silicon is longest but is limited by the film thickness.

The extent of the size effect depends on the film thickness relative to the phonon mean free path, but the free paths of phonons can be averaged in many ways and depend on particle energy. Consequently, the literature contains differing values for the phonon mean free path in silicon. Based on results from kinetic theory given by

Eq. (1), the mean free path in bulk silicon at 300 K is approximately $\Lambda = 43$ nm with $C = \rho c_p = 1.64 \cdot 10^6$ J/m^{3}K, $k = 148$ W/m $\cdot$ K, and $v_s = 6533$ m/s. This value represents a lower bound for the mean free path because it ignores phonon dispersion. A BTE model fit to experimental data for single-crystal films yields a room-temperature effective mean free path of approximately 300 nm for the dominant phonons [13]. These examples illustrate that cited values for the phonon mean free path strongly depend on the calculation method.

Experimental and theoretical thermal conductivity and phonon mean free path results for thin silicon films indicate that bulk values overestimate heat conduction, possibly leading to large errors in device simulations. Asheghi et al. [12] recommend that thermal simulations of SOI transistors with device layers thicker than about 1.5 μm may use values for bulk thermal conductivity at room temperature and above. Experimental data demonstrates a thermal conductivity reduction of nearly 50% compared to the bulk value for 74 nm thick films [13], and modeling results predict that the reduction could exceed 50% for films thinner than 100 nm and 70% for films thinner than 50 nm at room temperature [24].

4.1 Modeling Phonon-Boundary Scattering

Thermal conductivity models of silicon films must include phonon boundary scattering to predict the size effect. One approach is to incorporate an additional scattering rate [44] into a BTE solution using Matthiessen's rule in Eq. (7). This effectively treats boundary scattering as a volumetric effect [71].

$$\frac{1}{\tau_{\text{boundary}}} = \frac{v_s}{d}\left(\frac{1-p}{1+p}\right). \tag{8}$$

The average phonon group velocity is v_s, d is the film thickness, and p is the degree of specularity, which represents the probability of specular phonon reflection from the sample boundary ($0 \le p \le 1$). A value of $p = 0$ corresponds to an entirely rough surface that diffusely, or randomly, scatters all incident phonons according to its surface temperature, similar to a blackbody emitting absorbed radiation. This effectively thermalizes the phonons, such that they contribute to the equilibrium phonon distribution. For $p = 0$, the scattering rate in Eq. (8) reduces to the rate at which phonons strike the film boundaries, while $p = 1$ designates a perfectly smooth surface that completely reflects all incoming phonons. Specularly reflected phonons travel back and forth between the specimen walls before they are internally scattered by other processes, analogous to the flow of a rarefied gas in a tube. Since there is no thermal resistance in this case, the boundary scattering rate is zero, as for a bulk material. The following expression for p is strictly valid only for normally incident phonons [44] but is commonly incorporated in boundary scattering models for silicon films,

$$p = \exp\left[-\pi\left(\frac{2\eta\omega}{v_s}\right)^2\right]. \tag{9}$$

Table 1 Summary of experimental data for the room-temperature thermal conductivity of single-crystal silicon films and nanowires

Investigators	Film thickness	Doping	Temperature range (K)	Measurement method	k (W/m · K) at 300 K
Savvides and Goldsmid [53, 67]	14.0, 18.6, 48.6, 98.4 μm	intrinsic	200 – 300	Si crystal placed between Bi_2Te_3 samples, temperature gradient through total sample depends on Si thermal conductivity	138, 140, 144, 146
Yu et al. [68]	4 μm	intrinsic	300	Diffusivity measured using thermal wave technique	128
Asheghi et al. [14]	3 μm	intrinsic P: $1.0 \cdot 10^{17}$, $1.0 \cdot 10^{18}$, $3.0 \cdot 10^{19}$ cm^{-3} B: $1.0 \cdot 10^{17}$, $1.0 \cdot 10^{18}$, $1.0 \cdot 10^{19}$ cm^{-3}	20 – 320	Steady-state Joule heating and electrical resistance thermometry for a suspended Si membrane	133 133, 121, 113 128, 119, 107
Asheghi et al. [12,24]	0.42, 0.83, 1.60 μm 0.42, 0.72, 1.42 μm	intrinsic	20 – 300	Steady-state Joule heating and electrical resistance thermometry for Si in an SOI wafer	88, 98, 138 101, 128, 141

Zheng et al. [25]	155 nm	intrinsic	300	Steady-state Joule heating and electrical resistance thermometry for silicon suspended in a microbridge	2.2	
Ju and Goodson [13]	74 – 240 nm	intrinsic	300	Periodic Joule heating using patterned aluminum bridges of varying widths for Si in an SOI wafer	74.7 – 101	
Völklein [15]	75 nm	As: $3 \cdot 10^{19}$, $6 \cdot 10^{19}$, $2 \cdot 10^{20}$ cm^{-3}	100 – 350	Steady-state Joule heating and electrical resistance thermometry in a suspended Si membrane		61.8, 42.8, 13.1
		B: $3 \cdot 10^{19}$, $6 \cdot 10^{19}$ cm^{-3}				54.0, 17.7
	174 nm	As: $3 \cdot 10^{19}$, $6 \cdot 10^{19}$ cm^{-3}				82.0, 67.1
		B: $3.2 \cdot 10^{19}$, $6 \cdot 10^{19}$ cm^{-3}				61.9, 56.2
Li et al. [70]	nanowires: 22, 37, 56, 115 nm	intrinsic	20 – 320	Steady-state Joule heating and electrical resistance thermometry in platinum heaters supporting suspended nanowire	6.7, 17.2, 25.7, 40.5	

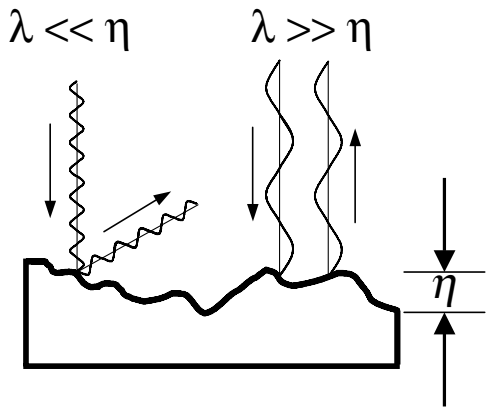

Figure 6 An illustration of phonons scattering on a rough surface (adapted from [44]). The root-mean-square surface roughness is indicated by η, and the phonon wavelength is λ.

Figure 6 illustrates the influence of phonon frequency ω and average surface roughness η on p. A surface or interface appears rough for phonon wavelengths shorter than the average surface roughness height but smooth for phonon wavelengths much longer than the surface roughness. A given surface may diffusely reflect high-frequency phonons and specularly reflect low-frequency phonons.

An alternative approach accounts for the mean free path reduction along a free-standing film by incorporating phonon scattering at the surfaces as boundary conditions for the BTE, resulting in an exact solution [72]. The overall relaxation time in the absence of boundary scattering τ_{bulk} is multiplied by a boundary scattering reduction factor F, which depends both on the ratio of film thickness to phonon mean free path $\delta = d/\Lambda$ and on the probability of specular reflection p given in Eq. (9),

$$\tau_{\text{layer}} = \tau_{\text{bulk}} F(\delta, p) = \tau_{\text{bulk}} \left[1 - \frac{3(1-p)}{2\delta} \int_1^\infty \left(\frac{1}{z^3} - \frac{1}{z^5} \right) \frac{1 - \exp(-\delta z)}{1 - p \exp(-\delta z)} dz \right]. \quad (10)$$

Integration requires the dummy variable z. This expression was derived for electrical conduction in metal films but is also valid for phonon heat transport.

Theoretical studies implementing these boundary scattering models have quantitatively explored the size effect in films. The BTE with the Debye and relaxation time approximations calculated the thermal conductivity of 0.42, 0.83, and 1.6 μm silicon films from 20 to 300 K [24] without any free fitting parameters by incorporating empirical scattering rates for bulk silicon [11] and Eq. (10) with $p = 0$ to account for boundary scattering. The predictions match the data reasonably well for temperatures down to about 100 K, below which the model overestimates the thermal conductivity reduction due to the assumption of entirely diffuse boundary scattering. Including partially diffuse scattering at the film boundaries using Eq. (9) for p with boundary roughness η as an adjustable parameter allows a better fit to this data [12],

most noticeably at low temperatures where boundary scattering dominates. Thermal conductivity calculations using the identical model are in good agreement with temperature-dependent data for a 3 μm film [14] and room-temperature values for 74 – 240 nm films [13]. A phonon Monte Carlo simulation [47] set p to a constant value of 0.6, chosen to best fit data over the entire temperature range for the 3 μm film.

These models indicate that specular boundary scattering in silicon films can be neglected at room temperature but is significant at low temperatures. The explanation is as follows. At low temperatures, the excited phonon modes tend to have low frequencies and long wavelengths, so a boundary appears smooth and specularly reflects some phonons. At higher temperatures, phonons occupy the more energetic modes with high frequencies and short wavelengths, so the effectively rough boundary diffusely scatters most phonons. It is usually not necessary to include partially specular boundary scattering in room-temperature thermal conductivity simulations.

At low temperatures, for which partially specular reflection is important, the degree of specularity p varies significantly depending on sample preparation. This is shown by Klistner et al. [54], who compared thermal conductance data for both rough and highly-polished silicon specimens of square cross-section at temperatures below 100 K. The mean free path in the rough samples was nearly identical to the smallest dimension, indicating mainly diffuse boundary scattering, while the highly polished samples had mean free paths four times longer, suggesting a high degree of specular reflection. Models of this data using Monte Carlo methods [54] and the equation of phonon radiative transfer [41] demonstrate that the phonon mean free path decreases as the probability of diffuse scattering increases. This is consistent with conclusions from thermal boundary resistance models of phonon transmission through interfaces, which is treated extensively in other texts [73].

4.2 Closed-Form Expressions

Since the full BTE can be practically expensive to solve, closed-form expressions are convenient for computing approximate thermal conductivity values.

For films much thicker than the phonon mean free path $\delta = d/\Lambda \gg 1$ and assuming entirely diffuse boundary scattering ($p = 0$), Eq. (10) reduces to a simple formula for the overall scattering rate in a film τ_{film}^{-1} [72]

$$\frac{1}{\tau_{\text{film}}} = \frac{1}{\tau_{\text{bulk}}} + \frac{3}{8}\frac{v_s}{d}, \tag{11}$$

where τ_{bulk}^{-1} is the overall scattering rate for bulk silicon and v_s is the phonon group velocity. This is, effectively, Matthiessen's rule with the overall film scattering rate given by a weighted sum of the rates for bulk silicon and for boundary scattering in Eq. (8). Substituting Eq. (11) into the kinetic theory expression from Eq. (1) with $\Lambda = v_s\tau$ results in the thermal conductivity k_{film} for a film of thickness d given its

corresponding bulk thermal conductivity value k_{bulk} [74]

$$k_{\text{film}} = \frac{(1/3)Cv}{(1/3)Cv/k_{\text{bulk}} + 3/(8d)}, \tag{12}$$

$$\frac{1}{3}Cv = 1.13 \cdot 10^{13} \frac{\exp(195/T)}{T^2 \left(\exp(195/T) - 1\right)^2}. \tag{13}$$

Alternatively, if the film thickness is much less than the mean free path $\delta = d/\Lambda \ll 1$, Eq. (10) again reduces to a simple expression [72] that can be solved for the film thermal conductivity

$$k_{\text{film}} = (1/3)Cv\frac{3d}{4}\log\left(\frac{k_{\text{bulk}}}{(1/3)Cvd}\right), \tag{14}$$

using Eq. (13) for $Cv/3$.

Yet another thermal conductivity model for single-crystal silicon films uses a least-squares fit to the available film data. The thermal conductivity should approach the bulk value as the film thickness increases and is seen to vary inversely with the square root of the film thickness below approximately 100 μm [53]. This results in the following empirical equation.

$$k_{\text{film}} = -\frac{23.8}{\sqrt{d}} + 148. \tag{15}$$

The plot of thermal conductivity as a function of film thickness or nanowire diameter in Figure 7 compares experimental data for undoped silicon films and nanowires with predictions from these three closed-form models. The values calculated using Eq. (12) agree reasonably well with the data for films thicker than approximately 250 nm, but this model underestimates the measured thermal conductivity of thinner films. This implies that the assumption of a "thick" film ($\delta = d/\Lambda \gg 1$) is no longer valid, suggesting that the mean free path of bulk silicon may be less than 250 nm at room temperature. While the results predicted by Eq. (14) for films much thinner than the room-temperature mean free path also fall well below the film thermal conductivity data, they agree well with values for the three thickest nanowires. The empirical expression in Eq. (15) lies within most of the error bars for the film data, even for the films thinner than 250 nm.

4.3 Quantum Effects

While classical phonon boundary scattering reduces thermal conductivity in silicon films, quantum effects, such as phonon confinement, may also influence heat conduction in very thin films and nanowires by altering the phonon spectra and density of states. A silicon quantum-well model [19] based on the BTE including Umklapp, impurity, and boundary scattering and accounting for the dispersion of spatially confined acoustic phonons predicts that phonon confinement reduces the group velocity

compared to the bulk and affects relaxation times, leading to a large reduction in lattice thermal conductivity. For a 155 nm wide silicon quantum well at 300 K, this model predicts a thermal conductivity of 66.7 $W/m \cdot K$, underestimating the measured value of 87 $W/m \cdot K$ for a 150 nm film [13]. Thermal conductivity data for 74 – 240 nm films [13] exhibit a weaker dependence on film thickness at room temperature than the large size effect due to phonon confinement, suggesting it is not significant for these films.

In contrast, the thermal conductivity data for individual silicon nanowires plotted in Figure 4 shows that the low-temperature behavior of the 37 nm wire and, to a much greater extent, the 22 nm wire deviates from the T^3 dependence discussed in Section 3. This implies that effects in addition to boundary scattering may influence heat conduction for nanowires of these diameters [70]. A theoretical study of nanowire thermal conductivity [75] demonstrates that the Holland model [11] for silicon thermal conductivity discussed in Section 3 does not qualitatively match this data, possibly due to linearization of the phonon dispersion relations and inaccurate forms of the anharmonic scattering rates. Computing phonon dispersion from known interatomic potentials results in a much better fit [75], but neither the resulting dispersion relations nor the extent of any phonon confinement is reported.

In a separate study, calculations for a freestanding silicon nanowire 20 nm in diameter [76] show that spatial confinement modifies the acoustic phonon dispersion and reduces the average group velocity by a factor of two compared to bulk silicon. This is in general agreement with Raman spectroscopy measurements of silicon nanowires, which indicate that phonon confinement becomes significant for

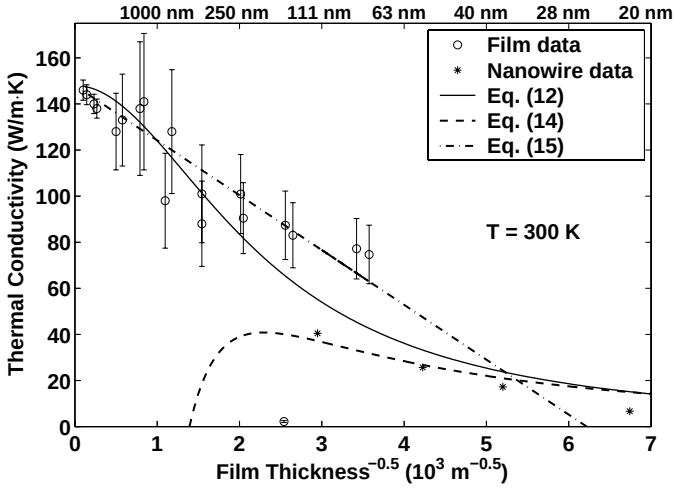

Figure 7 Experimental data of silicon thermal conductivity as a function of film thickness or nanowire diameter at room temperature plotted with the closed-form models of Eq. (12) [74] and of Eq. (14) and the least-squares fit from Eq. (15).

nanowires of diameter less than 22 nm [77]. Incorporating the modified dispersion relations into a BTE model of silicon [76] demonstrates that phonon confinement prevents the thermal conductivity from recovering its bulk value even with entirely specular boundary scattering. Phonon scattering rates that strongly depend on the group velocity, such as impurity scattering in Eq. (16), are also affected. With purely diffuse boundary scattering and full phonon confinement, the model predicts that the nanowire thermal conductivity drops to 9% of the bulk value. This represents a lower bound for thermal conductivity, since a nanowire embedded in a surrounding material may have only partially confined acoustic phonons [76].

MD simulations of silicon nanowire thermal conductivity show a nearly two orders of magnitude reduction and an increase with nanowire cross-sectional area [61], but they do not resolve whether the dominant mechanism is the modified phonon spectrum or a higher rate of diffuse boundary scattering. An EPRT model without phonon confinement indicates that for a given characteristic dimension, a circular silicon nanowire has the lowest thermal conductivity, followed by a square cross section nanowire, and then a film with in-plane heat transport [55]. A circular cylinder has the largest surface-to-volume ratio and thus the most boundary scattering and the strongest thermal conductivity reduction, while an infinite two-dimensional film experiences the least scattering.

5 DOPED SILICON FILMS

Doping alters silicon thermal conductivity, since the scattering of phonons on the dopant atoms in the lattice reduces the effective phonon conductivity. Additionally, scattering on free electrons associated with the dopant atoms can significantly reduce the phonon conductivity at low temperatures below the maximum thermal conductivity [45]. As an illustration, Figure 8 presents temperature-dependent data for boron in single-crystal silicon. Compared to intrinsic bulk silicon [7], lightly-doped (10^{16} cm^{-3}) bulk silicon [78] exhibits reduced thermal conductivity at temperatures below approximately 100 K with a lower peak value shifted to a higher temperature. Impurity scattering affects thermal conductivity in this regime, since Umklapp scattering dominates at higher temperatures as discussed in Section 3. The thermal conductivity of heavily doped (10^{20} cm^{-3}) bulk silicon [43] is much lower than intrinsic bulk values for all temperatures below 300 K and is a factor of three smaller at room temperature. A likely cause is phonon-electron scattering, which is insignificant for lightly doped semiconductors [76], but may achieve a similar rate as Umklapp and impurity scattering at very high doping concentrations.

Data for 3 μm films [14] plotted in Figure 8 shows that boron doping concentrations of 10^{17} cm^{-3} and less do not perceptibly affect the thermal conductivity at any temperature compared to an intrinsic film of identical thickness. This indicates that boundary scattering outweighs the effects of impurity scattering until the high-temperature regime, where Umklapp scattering still dominates. In contrast, doping concentrations of 10^{18} and 10^{19} cm^{-3} reduce the thermal conductivity at temperatures

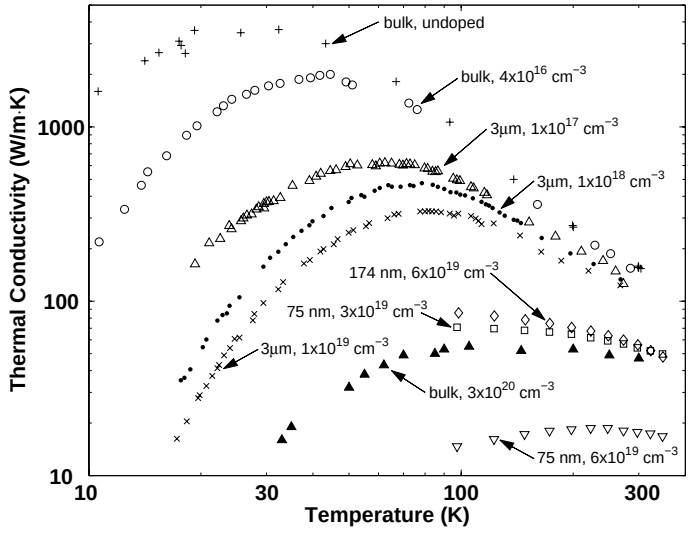

Figure 8 Thermal conductivity of boron-doped silicon as a function of temperature, showing the effects of doping concentration and film thickness. Experimental data come from the literature for undoped bulk silicon [7], lightly doped bulk silicon [78], heavily doped bulk silicon [43], the 3 μm films [14], and the 174 and 75 nm films [15].

below approximately 200 K and shift the peak to higher temperatures. The thermal conductivity of each 3 μm film approaches the bulk value near room temperature.

Temperature-dependent data in Figure 8 for 174 and 75 nm films doped with varying concentrations of boron [15] shows that higher doping levels lead to greater thermal conductivity reductions. Unlike the 3 μm samples, these thinner films all have much lower values than bulk intrinsic silicon at room temperature as shown in Figure 7. This is mainly due to strong boundary scattering, since intrinsic films of similar thickness also have substantially lower thermal conductivity than the bulk. The experimental data suggest that boundary scattering in very thin films outweighs some effects of impurity scattering, such that a doping level that reduces bulk thermal conductivity may not affect the film.

Dopant species affect silicon thermal conductivity depending on how their physical properties influence relevant scattering rates. The impurity scattering rate is proportional to the square of the mass difference between the host (silicon) and dopant atoms ΔM and to the dopant concentration n [44].

$$\frac{1}{\tau_{\text{impurity}}} = \frac{nV^2\omega^4}{4\pi v_s^3}\left(\frac{\Delta M}{M}\right)^2. \tag{16}$$

The volume of the host (silicon) atom is denoted by V, v_s is the average phonon group velocity, M is the silicon atomic mass, and ω is the phonon frequency. The mass differences between silicon and phosphorus, boron, and arsenic atoms are 2.89,

17.27, and 46.84 g/mol, respectively. Therefore, arsenic is expected to cause the largest thermal conductivity reduction followed by boron and then phosphorus for a given doping concentration. Figure 9 demonstrates that a 3μm thick boron-doped film has lower thermal conductivity than a phosphorus-doped film with the same impurity concentration. However, arsenic-doped films of thickness 75 and 174 nm have larger values than boron-doped films of identical doping concentration. One explanation may be dopant segregation to the interface between the silicon film and the underlying silicon dioxide layer in the experimental structure. A silicon-oxide interface traps up to 34% of an implanted arsenic dose during annealing, and the captured dopants are electrically inactive and immobile [79]. If this reduces the effective arsenic doping concentration by a factor of three, the impurity scattering rate for arsenic is still 2.5 times stronger than for boron. This suggests that additional phenomena, possibly including electron-phonon scattering, are significant. The electron-phonon scattering rate is proportional to the square of the deformation potential [80, 81], which varies according to whether the dopant is n- or p-type [44]. If the deformation potential for boron is larger than for arsenic, electron-phonon scattering in the boron-doped film would be stronger, but the extent of this scattering mechanism is unclear. Figure 9 shows that the room-temperature thermal conductivity for the 75 and 174 nm films with both boron and arsenic doping is lower than for intrinsic films 74 and 150 nm thick, indicating that boundary scattering alone does not account for this reduction. Impurity scattering is probably not significant at room temperature, but there is insufficient experimental data to make conclusive statements about the strength of electron-phonon scattering.

6 POLYSILICON FILMS

In contrast to single-crystal silicon, polycrystalline silicon contains grain boundaries that scatter phonons and reduce thermal conductivity. The transmission probability for phonons through grain boundaries depends on the relative orientations of the bounding crystals and on the concentration of related defects near the boundary [82]. Processing conditions affect polysilicon microstructure, particularly the grain size, grain structure, and defect density, making experimental data on well-characterized samples invaluable for predicting the thermal conductivity of polysilicon films.

Polysilicon microstructure depends on the fabrication method. The two main polysilicon deposition techniques are low-pressure chemical vapor deposition (LPCVD) and sputtering, but LPCVD is prevalent mainly due to its superior coverage of steep surfaces [42]. Experimental studies of LPCVD polysilicon [83–91] show that grain structure depends primarily on the deposition temperature and any postdeposition heat cycles. Silicon deposition usually occurs between 525°C and 650°C, and the resulting film is amorphous for temperatures below approximately 570 – 600°C, but is polycrystalline with a columnar grain structure at higher temperatures [42]. In a columnar structure, many grains span the entire film thickness, and the average size at the top film surface is larger than at the bottom. Annealing an amorphous silicon film between 600°C and 1000°C converts it to a poly-

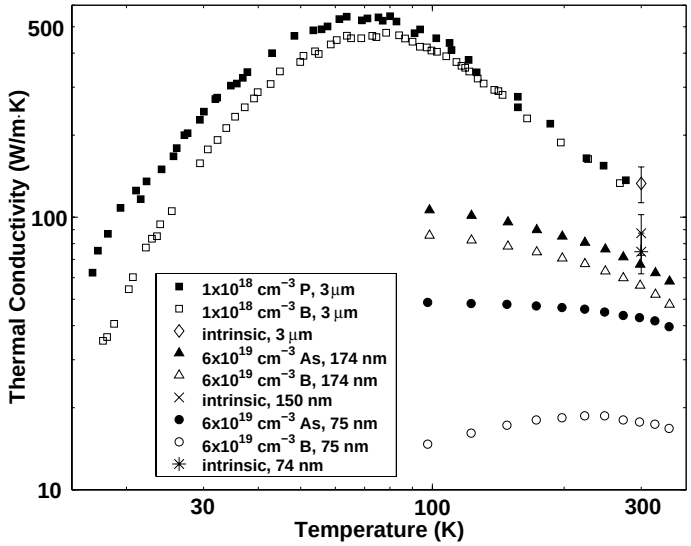

Figure 9 Thermal conductivity as a function of temperature, comparing the effect of n- and p-type dopants at constant doping concentrations on silicon films of thickness 3 μm [14] and 174 and 75 nm [15]. Values for 3 μm [14] and 150 and 74 nm [13] intrinsic silicon films at 300 K demonstrate the effect at room temperature.

crystalline form, but recrystallized polysilicon does not have a columnar structure because grains nucleate and grow above and below each other [42]. Figures 10a and 10b contain cross-sectional TEM images of a columnar grain structure in as-deposited polysilicon and of a random structure in amorphous recrystallized polysilicon, respectively. The average LPCVD polysilicon grain size increases with deposition temperature, and annealing causes additional grain growth, with the final grain

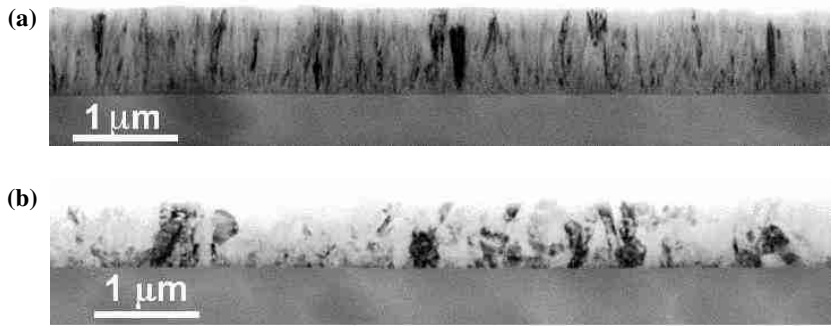

Figure 10 Cross-sectional TEM images of LPCVD polysilicon [17]: (a) Columnar grain structure of polysilicon deposited at 620°C and (b) Random grain structure of amorphous silicon deposited at 525°C and annealed at 900°C for one hour to form polysilicon.

size depending on the temperature, duration [4], and type (furnace or rapid thermal anneal) [91]. Grains in amorphous silicon nucleate and grow faster than columnar grains in as-deposited polysilicon, such that a recrystallized grain size can exceed that of annealed polysilicon [42].

Doping polysilicon affects grain size and phonon scattering and occurs either during deposition by adding dopant gases to silane, or after deposition using diffusion or ion implantation [42]. Temperatures of the diffusion doping process and of the anneal following ion implantation needed to activate the dopants and repair damage to the crystal lattice influence grain growth, with higher temperatures generally resulting in larger grain sizes [92]. N-type dopants, such as arsenic and phosphorus, significantly enhance grain growth, while p-type dopants including boron have only a minimal effect [83]. Phosphorus and arsenic concentrations greater than $4 \cdot 10^{20}$ cm^{-3} [84] and $1 \cdot 10^{19}$ cm^{-3} [42], respectively, most substantially increase the growth rate. Dopant atoms and their associated free electrons or holes also contribute to phonon scattering [44]. P-type dopants, such as boron, are uniformly distributed within the grains, while n-type dopants including arsenic and phosphorus tend to migrate to the grain boundaries in polysilicon [93].

Table 2 summarizes polysilicon experimental data, and Figure 11 plots temperature-dependent thermal conductivity for intrinsic polysilicon films. The three as-grown films in Figure 11 were deposited as polysilicon at 620°C with a columnar grain structure [17, 34], while the recrystallized film was deposited as amorphous silicon

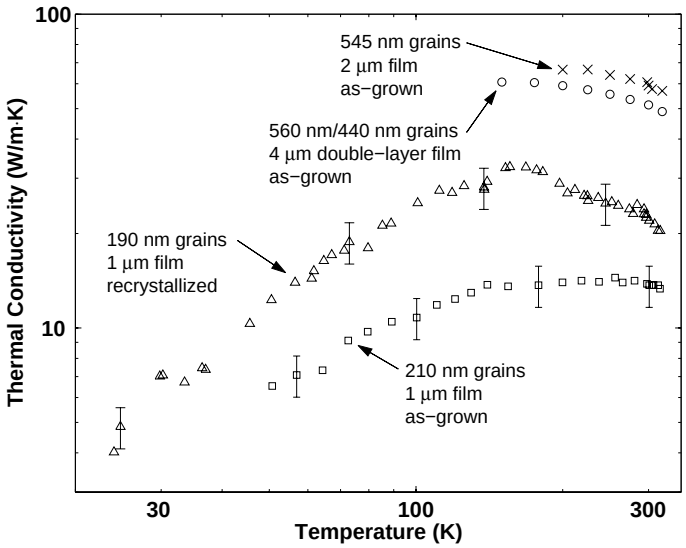

Figure 11 Thermal conductivity data as a function of temperature for undoped polysilicon films [17, 34]. The average grain size, film thickness, and deposition method are given for each data set. The double-layer film comprises two films of 2 μm thickness with different average grain sizes as indicated on the plot.

at 525°C and then annealed at 900°C for 1 hr to allow recrystallization with randomly oriented grains. The data for as-grown polysilicon indicate that larger grains result in higher thermal conductivity values. This conclusion is consistent with a study of LPCVD polysilicon given in Table 2, which found that both grain size and room-temperature thermal conductivity increase with deposition temperature from 590 to 630°C [39]. The low out-of-plane thermal conductivity value of 0.97 $W/m \cdot K$ listed in Table 2 for 2.2, 4.9, and 9.9 μm sputtered polysilicon films probably results from the small grain size of 300 Å [94]. Grain structure also appears to be important, since the recrystallized film in Figure 11 has higher thermal conductivity than the 1 μm as-grown film despite a slightly smaller grain size. The grain size for the as-grown films refers to the average at the top surface, while the recrystallized grain size is valid throughout the thickness. Columnar grains become smaller toward the bottom surface, reducing the thermal conductivity of the as-grown film.

Figure 12 presents temperature-dependent thermal conductivity for doped polysilicon. Quantitatively comparing the different data sets is difficult since important parameters affecting the thermal conductivity, including the grain size, the dopant species and concentration, and the film deposition temperature, are not all available. Some studies [16, 27, 30] estimate the carrier concentration through Hall effect measurements, but exact impurity concentrations cannot be determined from this infor-

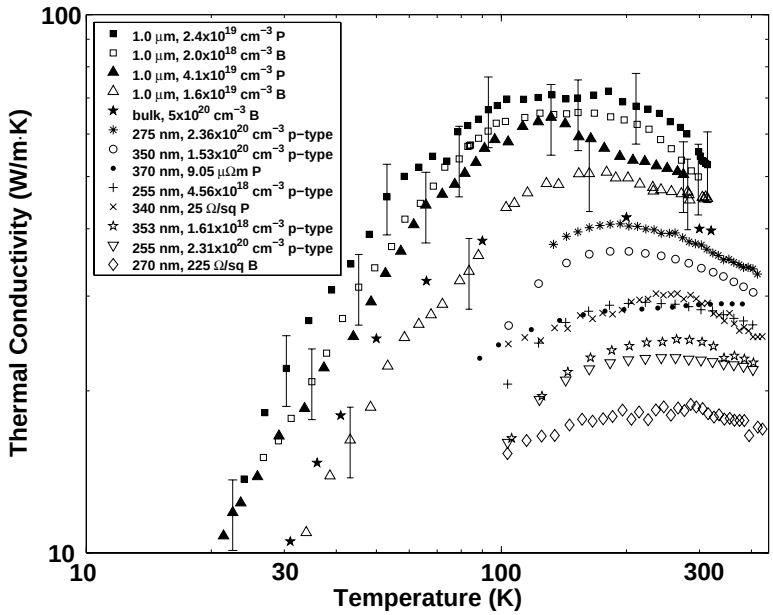

Figure 12 Thermal conductivity data as a function of temperature for doped polysilicon [16, 18, 28, 30, 43]. The legend indicates film thickness, dopant species or type, and dopant or carrier concentration or electrical resistivity, as available. Table 2 lists additional details.

Table 2 Summary of experimental data for the room-temperature thermal conductivity of polysilicon films

Investigators	Film deposition technique	Film thickness	Doping	Temperature range (K)	Measurement method	k (W/m·K) at 300 K
Wei et al. [39]	LPCVD, 590 – 630°C	0.7 – 1.6μm	intrinsic	300	Diffusivity measured using thermal wave technique	15 – 23
Uma et al. [17]	LPCVD, 620°C (as-grown) / LPCVD, 525°C (recrystallized)	1 μm	intrinsic	20 – 320	Steady-state Joule heating in a suspended membrane	13.8 / 22.0
Henager and Pawlewicz [94]	sputtering	2.2, 4.9, 9.9 μm	intrinsic	300	Thermal comparator technique	0.97
Graham [34]	LPCVD, 620°C	2 μm / 4 μm	intrinsic	200 – 320 / 150 – 320	Steady-state Joule heating in a suspended membrane	59.2 / 51.4
Tai et al. [31, 32]	LPCVD	1.5 μm	P diffusion	300 – 425	Steady-state current-voltage characteristics of microbridge	32
Mastrangelo et al. [100]	LPCVD, 650°C	1.3 μm	P diffusion	300	Diffusivity measured using AC heating of microbridge	27.9

Völklein and Baltes [30]	Commercial CMOS process	370 nm	P: 9.05 $\mu\Omega m$	80 – 400	Steady-state Joule heating in a differential microcantilever structure	29
Paul and Baltes [28, 29]	Commercial CMOS process	340 nm 270 nm	P: 25 Ω/□ B: 225 Ω/□	100 – 420	Steady-state Joule heating in a differential micro-cantilever structure	29 18
Paul et al. [27]	Commercial CMOS processes	not reported	n- and p-type: $4.0 \cdot 10^{18} - 3.4 \cdot 10^{20}$ cm^{-3}	300	Steady-state Joule heating in a differential micro-cantilever structure	16 – 24
Von Arx et al. [16]	Commercial CMOS processes	255 – 353 nm	p-type: $4.56 \cdot 10^{18} - 2.36 \cdot 10^{20}$ cm^{-3}	100 – 400	Steady-state Joule heating in a differential microcantilever structure	22.4 – 37.3
Irace and Sarro [33]	LPCVD	300 nm	B: $1 \cdot 10^{15}$ cm^{-2} and 40 keV	300	Steady-state Joule heating in a suspended membrane, thermocouples	34.5
McConnell et al. [18]	LPCVD, 620°C	1 μm	P: $2.4 \cdot 10^{19}$ cm^{-3} P: $4.1 \cdot 10^{19}$ cm^{-3} B: $2.0 \cdot 10^{18}$ cm^{-3} B: $1.6 \cdot 10^{19}$ cm^{-3}	20 – 320	Steady-state Joule heating in a suspended membrane	57.5 49.1 49.4 45.6

mation due to carrier trapping at the grain boundaries [87]. For a given dopant species, higher dopant concentrations should result in lower thermal conductivity values since the larger numbers of impurities provide more phonon scattering sites. The 1.0 μm films doped with phosphorus and boron exhibit this behavior. For a given dopant concentration, a phosphorus-doped film should have higher thermal conductivity than a boron-doped film. A fraction of n-type atoms collects at the grain boundaries in polysilicon, so phosphorus doping creates fewer scattering sites within the grains. From Eq. (16), impurity scattering for phosphorus is nearly 36 times smaller than for boron due to the varying mass differences. Comparing the 1.0 μm data, the thermal conductivity of both phosphorus-doped films exceeds that of the film doped with the highest boron concentration.

It is difficult to predict polysilicon thermal conductivity based on either electrical resistivity or doping concentration alone, since the grain size is also important. A study of bulk polysilicon doped with $5 \cdot 10^{20}$ cm^{-3} boron reports a room-temperature thermal conductivity of 40 W/m $\cdot$ K [43], which is surprisingly lower than values for some doped and undoped polysilicon films. The grain size must strongly influence the thermal conductivity of this sample, but no microstructural details are available. Data for 255 – 370 nm films in Figure 12 lie below that for the 1 μm films. Not only does increased scattering on the film boundaries decrease the phonon mean free path, but thinner films also require shorter anneal times to activate dopant atoms. This likely leads to smaller grains [34], augmenting the mean free path reduction. The combined effects of a thinner film, smaller grains, and in some instances more impurities result in lower thermal conductivity values.

Phonon scattering on grain boundaries depends on the grain size and structure [82]. The grain boundary scattering rate for lateral conduction in a film can be approximated using Eq. (8),

$$\frac{1}{\tau_{\text{grain}}} = \frac{v_s}{d_g}\left(\frac{1 - p_{tr}(\omega)}{1 + p_{tr}(\omega)}\right). \tag{17}$$

The grain size d_g is not necessarily the only critical parameter because the probability of phonon reflection at a grain boundary can depend on its roughness and on the density of defects near the boundary. These effects can be modeled using $p_{tr}(\omega)$ as the probability of specular transmission ($0 \leq p_{tr}(\omega) \leq 1$). Specular transmission at the grain boundaries increases the effective grain size. Assuming that grain boundary roughness dominates specular transmission, Eq. (9) with η as the RMS grain boundary roughness can estimate p_{tr}. The transmission probability should decrease with increasing phonon energy as the wavelength approaches the characteristic scales of boundary roughness and defects. Therefore, the scattering strength of grain boundaries in a given film can be expected to increase with increasing temperature [95]. A BTE model of doped polysilicon data found that the phonon mean free path exceeded the average grain size for temperatures below approximately 20 – 50 K [18].

A closed-form expression developed for doped polysilicon films [18] relates room-temperature thermal conductivity to grain size and to impurity concentration and type, all of which can be measured. From the scattering rates given in Eqs. (16)

and (17), thermal conductivity is nearly proportional to the average grain size d_g and inversely proportional to the impurity concentration n. The thermal conductivity of a 1.0 μm film at 300 K is approximated by

$$k(d_g, n) = \frac{1}{3} C_S v_s \left(\frac{A_1}{d_g} + A_2 n \right)^{-1}, \tag{18}$$

where $v_s = 6166$ m/s is the averaged phonon group velocity in silicon and $C_S = 1.654 \cdot 10^6$ J/m^{3}K is the phonon specific heat at 300 K in silicon. The constants in Eq. (18) are $A_1 = 2.887 \cdot 10^{10}$ nm/m and $A_2 = 3.200 \cdot 10^{-13}$ cm^3/m for boron and $A_1 = 2.887 \cdot 10^{10}$ nm/m and $A_2 = -1.122 \cdot 10^{-14}$ cm^3/m for phosphorous.

Figure 13 plots the temperature-dependent thermal conductivity for various silicon forms to qualitatively illustrate the impact of phonon scattering on dopant atoms and on grain and film boundaries. Compared to bulk single-crystal silicon, the maximum thermal conductivity of the single-crystal film is an order of magnitude smaller and shifted to a higher temperature due to boundary scattering. Impurity scattering reduces the thermal conductivity of the doped single-crystal film below approximately 100 K and again shifts the peak to a higher temperature. The room-temperature values converge for all three single-crystal samples, which is consistent with the fact that boundary and impurity scattering are most significant at lower temperatures. The doped polysilicon film has lower thermal conductivity than the single-

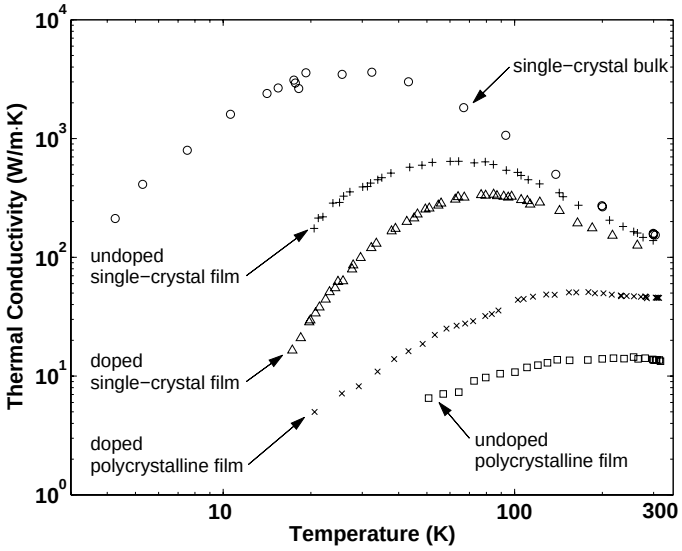

Figure 13 Comparison of temperature-dependent thermal conductivity data for various silicon samples (adapted from [18]): Undoped single-crystal bulk [8]: $d = 0.44$ cm; Undoped single-crystal film [14]: $d = 3$ μm; Doped single-crystal film [14]: $d = 3$ μm, $n = 1.0 \cdot 10^{19}$ cm^{-3}B; Doped polycrystalline film [18]: $d = 1$ μm, $n = 1.6 \cdot 10^{19}$ cm^{-3}B; $d_g = 408$ nm; Undoped polycrystalline film [17]: $d = 1$ μm, $d_g = 210$ nm.

crystal film doped with a comparable concentration at all temperatures, implying that grain boundary scattering dominates the thermal resistance of a polysilicon film at this dopant concentration. The doped polysilicon film exhibits higher thermal conductivity at all temperatures than the intrinsic polysilicon film. These films were deposited under identical conditions, but the doped film was annealed following ion implantation, which resulted in an average grain size nearly double that of the intrinsic film. Although dopant atoms provide additional phonon scattering sites, the difference in grain sizes has a much greater effect on the observed thermal conductivity.

7 HOTSPOTS IN NANOSTRUCTURES

Thermal conductivity is usually measured and calculated at locations far from the heat source, where the phonon system is always near equilibrium. This enables the use of classical theories such as the Boltzmann transport equation. However, the situation changes locally near heat sources smaller than the phonon mean free path, where non-equilibrium phonon transport dominates. Theoretical work has investigated the impact of small hotspots on localized heat conduction, but fabrication and measurement difficulties associated with the extremely small scale of these effects have limited experimental progress. Consequently, little data presently exist for nanoscale energy transport phenomena in silicon, making it difficult to verify modeling methods and predictions. Studies of nonequilibrium heating and quantum effects in silicon CMOS devices are relevant as device dimensions shrink, causing electric fields and volumetric power density to increase despite decreasing supply voltages [1].

Hotspots, or regions of intense phonon-electron coupling caused by energetic electrons out of thermal equilibrium with the silicon lattice, become significant for devices with channel lengths shorter than the phonon mean free path [3]. Few collisions take place with the surrounding lattice due to ballistic phonon emission from a hotspot, preventing the establishment of thermal equilibrium and leading to temperature rises above those predicted by diffusion theory [96]. For device technologies with channel lengths below 100 nm, typical hotspot dimensions are on the order of 10 nm [96], which is small compared to the room-temperature mean free path in silicon. Hotspots can arise due to electrostatic discharge (ESD) events but also tend to occur at the drain of FET devices where the electric field is highest [3, 97].

The coupling of electron and phonon scattering events and the decay of optical into acoustic phonons complicate the modeling and analysis of subcontinuum heating in silicon. Hot electrons produced at the drain of a typical device are very energetic and preferentially scatter with high-frequency optical phonons [96]. Due to their low group velocities and fast scattering rates, optical phonons move only a few nanometers before anharmonically decaying into faster acoustic phonons. The time scale for this process is about two orders of magnitude slower than for electron-optical phonon scattering owing to the weak coupling between optical and acoustic modes, so optical phonons create a heat conduction bottleneck by accumulating near

the hotspot. This impedes heat transport away from the hotspot region and causes intense localized heating, which can be sufficient to melt silicon [96]. In this way, hotspots govern the peak device temperature, and lattice heating affects temperature-dependent electron transport parameters that can alter device behavior and reliability [98].

Diffusion theory does not account for nonequilibrium heating effects, so alternate modeling approaches are necessary. A phonon BTE solution including boundary scattering for an SOI circuit with a 72 nm thick silicon device layer calculated a peak temperature rise nearly 160% higher than that predicted by diffusion theory [3]. The conducting channel carrying most of the electrical current was located within the top few nanometers of silicon below the gate, creating a heat generation region smaller

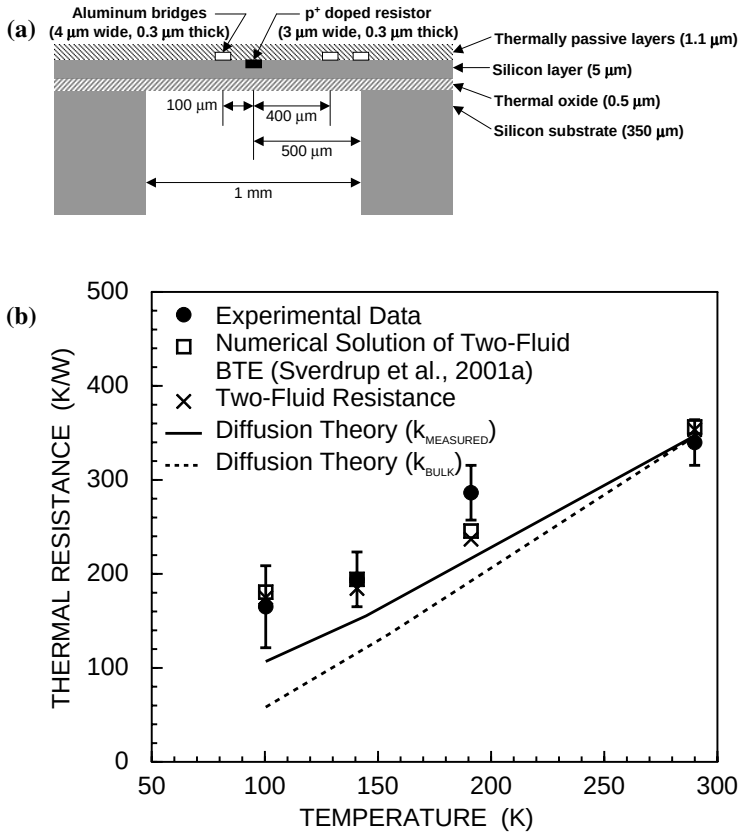

Figure 14 Experiment demonstrating subcontinuum heat transport effects in silicon near a hotspot with dimensions small relative to the acoustic phonon mean free path: (a) Schematic of the side view of the experimental structure (adapted from [20]); and (b) Data points with predictions based on diffusion theory, a detailed BTE analysis [3], and diffusion theory corrected to account for the decay of optical to acoustic phonons (adapted from [20]).

than the room-temperature phonon mean free path in silicon. Subcontinuum effects near a small heating source were experimentally detected with the suspended silicon membrane [20] shown in Figure 14a. This experimental structure is similar to the thermal conductivity measurement device in Figure 1, except the heater is a doped silicon resistor along the center of the membrane. Reverse biasing the surrounding silicon confines current to the doped region to create a Joule heated hotspot. The doped resistor temperature exceeds that predicted by diffusion theory, while the temperatures of the aluminum bridges, located many mean free paths from the hotspot, follow Fourier's law. The plot of silicon membrane thermal resistance in Figure 14b shows that the discrepancy between the measurements and diffusion theory is largest at the lowest temperatures where the mean free path is longest and diminishes with increasing temperature. At room temperature, the measurement agrees with diffusion theory since the mean free path is shorter than the hotspot size.

Diffusion theory cannot predict the temperature rise near a hotspot because it does not consider the thermal resistance associated with the decay from optical to acoustic phonons. This resistance scales as the square of the ratio of the mean free path to hotspot radius, resulting in a larger temperature rise at lower temperatures where the mean free path is longer [20]. Simplifying a phonon BTE solution that assigns different temperatures to the optical and acoustic phonons results in a thermal resistance between these two modes, which is effectively a correction to diffusion theory [98]. Figure 14b compares this model with the experimental data and other predictions. This thermal resistance becomes significant when a hotspot is small compared to the acoustic phonon mean free path and is much larger than the resistance due to optical phonon emission from the hotspot [98]. While these studies demonstrate and explain sub-continuum effects at low temperatures resulting from small heat generation regions, room-temperature data would be of great value for predicting the impact of hotspots on practical device operation.

8 CONCLUDING REMARKS

This article provides an overview of thermal conductivity data and theoretical studies for single-crystal and polycrystalline silicon. Experimental data indicate that phonon scattering at film boundaries reduces the thermal conductivity of thin films compared to bulk silicon. Grain boundary scattering in polysilicon controls the thermal conductivity at and below room temperature. Dopant atoms decrease silicon thermal conductivity most significantly below room temperature, and the extent of this reduction depends on the dopant species due to mass-difference scattering and dopant segregation to grain boundaries in polysilicon. Further investigation of quantum effects on the thermal conductivity of silicon nanostructures is required, as is additional experimental validation of existing models. In particular, more experimental data is required to probe the effects of nonequilibrium heating due to nanoscale hotspots, especially at and above room temperature to more accurately reflect the operating conditions of most practical devices.

REFERENCES

1. *Semiconductor Industry Association*, International Technology Roadmap for Semiconductors, http://public.itrs.net, 2001.
2. K. E.Goodson, M. I. Flik, L. T. Su, and D. A. Antoniadis, Prediction and Measurement of Temperature Fields in Silicon-on-Insulator Electronic Circuits, *J. Heat Transfer*, Vol. 117, pp. 574–581, 1995.
3. P. G. Sverdrup, Y. S. Ju, and K. E. Goodson, Sub-Continuum Simulations of Heat Conduction in Silicon-on-Insulator Transistors, *J. Heat Transfer*, Vol. 123, pp. 130–137, 2001.
4. S. M. Sze, *VLSI Technology*, McGraw-Hill, New York, 1988.
5. P. Vettiger, G. Cross, M. Despont, U. Drechsler, U. Durig, B. Gotsmann, W. Haberle, M. A. Lantz, H. E. Rothuizen, R. Stutz, and G. K. Binnig, The Millipede: Nanotechnology Entering Data Storage, *IEEE Trans. Nanotechnol.*, Vol. 1, pp. 39–55, 2002.
6. L. Jiang, M. Wong, and Y. Zohar, Micromachined Polycrystalline Thin Film Temperature Sensors, *Measurement Sci. Technol.*, Vol. 10, pp. 653–664, 1999.
7. C. J. Glassbrenner and G. A. Slack, Thermal Conductivity of Silicon and Germanium from 3 K to the Melting Point, *Phys. Rev.*, Vol. 134, pp. A1058–A1069, 1964.
8. Y. S. Touloukian, R. W. Powell, C. Y. Ho, and P. G. Klemens, *Thermal Conductivity of Metallic Elements and Alloys*, IFI/Plenum, New York, Vol. 1, 1970.
9. P. G. Klemens, The Thermal Conductivity of Dielectric Solids at Low Temperatures, *Proc. Roy. Soc. London, Ser. A*, Vol. 208, pp. 108–133, 1951.
10. J. Callaway, Model for Lattice Thermal Conductivity at Low Temperatures, *Phys. Rev.*, Vol. 113, pp. 1046–1051, 1959.
11. M. G. Holland, Analysis of Lattice Thermal Conductivity, *Phys. Rev.*, Vol. 132, pp. 2461–2471, 1963.
12. M. Asheghi, M. N. Touzelbaev, K. E. Goodson, Y. K. Leung, and S. S. Wong, Temperature-Dependent Thermal Conductivity of Single-Crystal Silicon Layers in SOI Substrates, *J. Heat Transfer*, Vol. 120, pp. 30–36, 1998.
13. Y. S. Ju and K. E. Goodson, Phonon Scattering in Silicon Films with Thickness of Order 100 nm, *Appl. Phys. Lett.*, Vol. 74, pp. 3005–3007, 1999.
14. M. Asheghi, K. Kurabayashi, R. Kasnavi, and K. E. Goodson, Thermal Conduction in Doped Single-Crystal Silicon Films, *J. Appl. Phys.*, Vol. 91, pp. 5079–5088, 2002.
15. F. Völklein, Characterization of the Thermal Properties of Bulk and Thin-Film Materials by Using Diagnostic Microstructures, in: *Symposium on Microtechnology in Metrology and Metrology in Microsystems*, Delft University of Technology, Delft, the Netherlands, 2000.
16. M. von Arx, O. Paul, and H. Baltes, Process-Dependent Thin-Film Thermal Conductivities for Thermal CMOS MEMS, *J. Microelectromech. Sys.*, Vol. 9, pp. 136–145, 2000.
17. S. Uma, A. D. McConnell, M. Asheghi, K. Kurabayashi, and K. E. Goodson, Temperature Dependent Thermal Conductivity of Undoped Polycrystalline Silicon, *Int. J. Thermophys.*, Vol. 22, pp. 605–616, 2001.
18. A. D. McConnell, S. Uma, and K. E. Goodson, Thermal Conductivity of Doped Polysilicon Layers, *J. Microelectromech. Sys.*, Vol. 10, pp. 360–369, 2001.

19. A. Balandin and K. L. Wang, Significant Decrease of the Lattice Thermal Conductivity due to Phonon Confinement in a Free-Standing Semiconductor Quantum Well, *Phys. Rev. B*, Vol. 58, pp. 1544–1549, 1998.
20. P. G. Sverdrup, S. Sinha, M. Asheghi, S. Uma, and K. E. Goodson, Measurement of Ballistic Phonon Conduction near Hotspots in Silicon, *Appl. Phys. Lett.*, Vol. 78, pp. 3331–3333, 2001.
21. K. E. Goodson and M. I. Flik, Solid Layer Thermal-Conductivity Measurement Techniques, *Appl. Mech. Rev.*, Vol. 47, pp. 101–112, 1994.
22. S. R. Mirmira and L. S. Fletcher, Review of the Thermal Conductivity of Thin Films, *J. Thermophys. Heat Transfer*, Vol. 12, pp. 121–131, 1998.
23. D. G. Cahill, K. Goodson, and A. Majumdar, Thermometry and Thermal Transport in Micro/Nanoscale Solid-State Devices and Structures, *J. Heat Transfer*, Vol. 124, pp. 223–241, 2002.
24. M. Asheghi, Y. K. Leung, S. S. Wong, and K. E. Goodson, Phonon-Boundary Scattering in Thin Silicon Layers, *Appl. Phys. Lett.*, Vol. 71, pp. 1798–1800, 1997.
25. X. Y. Zheng, S. Z. Li, M. Chen, and K. L. Wang, Giant Reduction in Lateral Thermal Conductivity of Thin Nitride/Silicon/Oxide Membrane Measured with a Suspended Micro Structure, in: *Micro-Electro-Mechanical Systems (MEMS): Microscale Thermal Phenomena in Electronic Systems, Proc. ASME Int. Mech. Eng. Congr. and Expos.*, ASME, New York, Vol. 59, pp. 93–98, 1996.
26. M. von Arx, O. Paul, and H. Baltes, Determination of the Heat Capactiy of CMOS Layers for Optimal CMOS Sensor Design, *Sens. Actuat. A*, Vol. 46–47, pp. 428–431, 1995.
27. O. Paul, M. von Arx, and H. Baltes, Process-Dependent Thermophysical Properties of CMOS IC Thin Films, in: *8th Int. Conf. on Solid-State Sensors and Actuators, and Eurosensors IX*, Stockholm, Sweden, 1995.
28. O. M. Paul, J. Korvink, and H. Baltes, Determination of the Thermal Conductivity of CMOS IC Polysilicon, *Sens. Actuat. A*, Vol. 41–42, pp. 161–164, 1994.
29. O. Paul and H. Baltes, Thermal Conductivity of CMOS Materials for the Optimization of Microsensors, *J. Micromech. Microeng.*, Vol. 3, pp. 110–112, 1993.
30. F. Völklein and H. Baltes, A Microstructure for Measurement of Thermal Conductivity of Polysilicon Thin Films, *J. Microelectromech. Sys.*, Vol. 1, pp. 193–196, 1992.
31. Y. C. Tai, C. H. Mastrangelo, and R. S. Muller, Thermal Conductivity of Heavily Doped Low-Pressure Chemical Vapor Depositied Polycrystalline Silicon Films, *J. Appl. Phys.*, Vol. 63, pp. 1442–1447, 1988.
32. Y. C. Tai, C. H. Mastrangelo, and R. S. Muller, Thermal Conductivity of Heavily Doped LPCVD Polysilicon, in: *IEDM'87*,1987.
33. A. Irace and P. M. Sarro, Measurement of Thermal Conductivity and Diffusivity of Single and Multilayer Membranes, *Sens. Actuat. A*, Vol. 76, pp. 323–328, 1999.
34. S. Graham, B. Olson, C. Wong, E. Piekos, A. D. McConnell, and K. Goodson, The Effects of Processing Conditions on the Thermal Conductivity of Polycrystalline Silicon Films, in: *Proc. IMECE'03*, Washington, DC, 2003.
35. D. G. Cahill, Thermal Conductivity Measurement from 30 to 750 K: The 3ω Method, *Rev. Sci. Instrum.*, Vol. 61, pp. 802–808, 1990.
36. Y. S. Ju, K. Kurabayashi, and K. E. Goodson, Thermal Characterization of

Anisotropic Thin Dielectric Films Using Harmonic Joule Heating, *Thin Solid Films*, Vol. 339, pp. 160–164, 1999.

37. K. Kurabayashi, M. Asheghi, M. Touzelbaev, and K. E. Goodson, Measurement of the Thermal Conductivity Anisotropy in Polyimide Films, *J. Microelectromech. Sys.*, Vol. 8, pp. 180–191, 1999.
38. K. E. Goodson and Y. S. Ju, Heat Conduction in Novel Electronic Films, *Ann.Rev. Mater. Sci.*, Vol. 29, pp. 261–293, 1999.
39. L. Wei, M. Vaudin, C. S. Hwang, G. White, J. Xu, and A. J. Steckl, Heat Conduction in Silicon Thin Films: Effect of Microstructure, *J. Mater. Res.*, Vol. 10, pp. 1889–1896, 1995.
40. C. Kittel, *Introduction to Solid State Physics*, Wiley, New York, 1996.
41. A. Majumdar, Microscale Heat Conduction in Dielectric Thin Films, *J. Heat Transfer*, Vol. 115, pp. 7–16, 1993.
42. J. D. Plummer, M. D. Deal, and P. B. Griffin, *Silicon VLSI Technology: Fundamentals, Practice and Modeling*, Prentice Hall, Upper Saddle River, NJ, 2000.
43. G. A. Slack, Thermal Conductivity of Pure and Impure Silicon, Silicon Carbide, and Diamond, *J. Appl. Phys.*, Vol. 35, pp. 3460–3466, 1964.
44. J. M. Ziman, *Electrons and Phonons*, Oxford University Press, Oxford, UK, 1960.
45. G. P. Srivastava, *The Physics of Phonons*, Adam Hilger, Bristol, UK, 1990.
46. C. Jacoboni and P. Lugli, *The Monte Carlo Method for Semiconductor Device Simulation*, Springer-Verlag, New York, 1989.
47. S. Mazumder and A. Majumdar, Monte Carlo Study of Phonon Transport in Solid Thin Films Including Dispersion and Polarization, *J. Heat Transfer*, Vol. 123, pp. 749–759, 2001.
48. R. B. Peterson, Direct Simulation of Phonon-Mediated Heat Transfer in a Debye Crystal, *J. Heat Transfer*, Vol. 116, pp. 815–822, 1994.
49. J. E. Parrott, The High Temperature Thermal Conductivity of Semiconductor Alloys, *Proc. Phys. Soc.*, Vol. 81, pp. 726–735, 1963.
50. K. C. Sood and M. K. Roy, Longitudinal Phonons and High-Temperature Heat Conduction in Germanium, *J. Phys.: Condensed Matter*, Vol. 5, pp. 301–312, 1993.
51. C. M. Bhandari and G. S. Verma, Role of Longitudinal and Transverse Phonons in Lattice Thermal Conductivity of Ga As and In Sb, *Phys. Rev.*, Vol. 140, pp. A2101–A2104, 1965.
52. P. G. Klemens, Theory of Lattice Thermal Conductivity: Role of Low-Frequency Phonons, *Int. J. Thermophys.*, Vol. 2, pp. 55–62, 1981.
53. N. Savvides and H. J. Goldsmid, The Effect of Boundary Scattering on the High-Temperature Thermal Conductivity of Silicon, *J. Phys. C: Solid State Phys.*, Vol. 6, pp. 1701–1708, 1973.
54. T. Klitsner, J. E. van Cleve, H. E. Fischer, and R. O. Pohl, Phonon Radiative Heat Transfer and Surface Scattering, *Phys. Rev. B*, Vol. 38, pp. 7576–7594, 1988.
55. X. Lu, W. Z. Shen, and J. H. Chu, Size Effect on the Thermal Conductivity of Nanowires, *J. Appl. Phys.*, Vol. 91, pp. 1542–1552, 2002.
56. X. Lu and J. H. Chu, Phonon Heat Transport in Silicon Nanowires, *Euro. Phys. J. B*, Vol. 26, pp. 375–378, 2002.
57. F. H. Stillinger and T. A. Weber, Computer Simulation of Local Order in Con-

densed Phases of Silicon, *Phys. Rev. B*, Vol. 31, pp. 5262–5271, 1985.
58. P. K. Schelling, S. R. Phillpot, and P. Keblinski, Comparison of Atomic-Level Simulation Methods for Computing Thermal Conductivity, *Phys. Rev. B*, Vol. 65, pp. 144306-1–1444306-12, 2002.
59. S. Volz and G. Chen, Lattice Dynamic Simulation of Silicon Thermal Conductivity, *Physica B*, Vol. 263–264, pp. 709–712, 1999.
60. S. G. Volz and G. Chen, Molecular-Dynamics Simulation of Thermal Conductivity of Silicon Crystals, *Phys. Rev. B*, Vol. 61, pp. 2651–2656, 2000.
61. S. G. Volz and G. Chen, Molecular Dynamics Simulation of Thermal Conductivity of Silicon Nanowires, *Appl. Phys. Lett.*, Vol. 75, pp. 2056–2058, 1999.
62. R. D. Mountain and R. A.MacDonald, A Molecular-Dynamics Study of Heat Flow in a Two-Dimensional Crystal, *Phys. Rev. B*, Vol. 28, pp. 3022–3025, 1983.
63. X. L. Feng, Z. X. Li, and Z. Y. Guo, Size Effect of Lattice Thermal Conductivity Across Nanoscale Thin Films by Molecular Dynamics Simulations, *Chinese Phys. Lett.*, Vol. 18, pp. 416–418, 2001.
64. X. L. Feng, Z. X. Li, X. G. Liang, and Z. Y. Guo, Molecular Dynamics Study on Thermal Conductivity of Nanoscale Thin Films, *Chinese Sci. Bull.*, Vol. 46, pp. 604–607, 2001.
65. J. R. Lukes, D. Y. Li, X.-G. Liang, and C.-L. Tien, Molecular Dynamics Study of Solid Thin-Film Thermal Conductivity, *J. Heat Transfer*, Vol. 122, pp. 536–543, 2000.
66. P. K. Schelling, S. R. Phillpot, and P. Keblinski, Phonon Wave-Packet Dynamics at Semiconductor Interfaces by Molecular-Dynamics Simulation, *Appl. Phys. Lett.*, Vol. 80, pp. 2484–2486, 2002.
67. N. Savvides and H. J. Goldsmid, Thermal Conductivity of Thin Crystals of Pure Silicon, *Phys. Stat. Sol. B*, Vol. 63, pp. K89–K91, 1974.
68. X. Y. Yu, L. Zhang, and G. Chen, Thermal-Wave Measurements of Thin-Film Thermal Diffusivity with Different Laser Beam Configurations, *Rev. Sci. Instrum.*, Vol. 67, pp. 2312–2316, 1996.
69. G. Chen and M. Neagu, Thermal Conductivity and Heat Transfer in Superlattices, *Appl. Phys. Lett.*, Vol. 71, pp. 2761–2763, 1997.
70. D. Li, Y. Wu, P. Kim, L. Shi, P. Yang, and A. Majumdar, Thermal Conductivity of Individual Silicon Nanowires, *Appl. Phys. Lett.*, Vol. 83, pp. 2934–2936, 2003.
71. C.-L. Tien and G. Chen, Challenges in Microscale Conductive and Radiative Heat Transfer, *J. Heat Transfer*, Vol. 116, pp. 799–807, 1994.
72. E. H. Sondheimer, The Mean Free Path of Electrons in Metals, *Adv. Phys.*, Vol. 1, pp. 1–42, 1952.
73. E. T. Swartz and R. O. Pohl, Thermal Boundary Resistance, *Rev. Mod. Phys.*, Vol. 61, pp. 605–668, 1989.
74. Y. S. Ju and K. E. Goodson, Size Effect on Thermal Conduction in Silicon-on-Insulator Devices under Electrostatic Discharge (ESD) Conditions, *Jap. J. Appl. Phys.*, Vol. 36, pp. L798–L800, 1997.
75. N. Mingo, L. Yang, D. Li, and A. Majumdar, Predicting the Thermal Conductivity of Si and Ge Nanowires, *Nano Lett.*, Vol. 3, pp. 1713–1716, 2003.
76. J. Zou and A. Balandin, Phonon Heat Conduction in a Semiconductor Nanowire, *J. Appl. Phys.*, Vol. 89, pp. 2932–2938, 2001.

77. R.-P. Wang, G.-W. Zhou, Y.-L. Liu, S.-H. Pan, H.-Z. Zhang, D.-P. Yu, and Z. Zhang, Raman Spectral Study of Silicon Nanowires: High-Order Scattering and Phonon Confinement Effects, *Phys. Rev. B*, Vol. 61, pp. 16827–16832, 2000.
78. M. G. Holland and L. J. Neuringer, The Effect of Impurities on the Lattice Thermal Conductivity of Silicon, in: *Proc. Int. Conf. on Physics of Semiconductors*, Institute of Physics and the Physical Society of London, pp. 474–481, 1962.
79. R. Kasnavi, Y. Sun, R. Mo, P. Pianetta, P. B. Griffin, and J. D. Plummer, Characterization of Arsenic Dose Loss at the Si/SiO_2 Interface, *J. Appl. Phys.*, Vol. 87, pp. 2255–2260, 2000.
80. J. M. Ziman, The Effect of Free Electrons on Lattice Conduction, *Philos. Mag.*, Vol. 1, pp. 191–198, 1956.
81. J. M. Ziman, The Effect of Free Electrons on Lattice Conduction, *Philos. Mag.*, Vol. 2, pp. 292, 1957.
82. K. E. Goodson, Thermal Conduction in Nonhomogeneous CVD Diamond Layers in Electronic Microstructures, *J. Heat Transfer*, Vol. 118, pp. 279–286, 1996.
83. L. Mei, M. Rivier, Y. Kwark, and R. W. Dutton, Grain-Growth Mechanisms in Polysilicon, *J. Electrochem. Soc.*, Vol. 129, pp. 1791–1795, 1982.
84. Y. Wada and S.Nishimatsu, Grain Growth Mechanism of Heavily Phosphorus-Implanted Polycrystalline Silicon, *J. Electrochem. Soc.*, Vol. 125, pp. 1499–1504, 1978.
85. V. P. Lesnikova, A. S. Turtsevich, V. Y. Krasnitsky, V. A. Emelyanov, O. Y. Nalivaiko, S. V. Kravtsov, and T. V.Makarevich, The Structure, Morphology and Resistivity of In Situ Phosphorous Doped Polysilicon Films, *Thin Solid Films*, Vol. 247, pp. 156–161, 1994.
86. M. Hendriks and C. Mavero, Phosphorus Doped Polysilicon for Double Poly Structures: I. Morphology and Microstructure, *J. Electrochem. Soc.*, Vol. 138, pp. 1466–1470, 1991.
87. E. G. Lee and H. B. Im, Effects of Microstructure and As Doping Concentration on the Electrical Properties of LPCVD Polysilicon, *J. Electrochem. Soc.*, Vol. 138, pp. 3465–3469, 1991.
88. N. G. Nakhodkin and T. V. Rodionova, Formation of Different Types of Polysilicon Film Structures and Their Grain Growth under Annealing, *Phys. Stat. Sol. A*, Vol. 123, pp. 431–439, 1991.
89. G. Harbeke, L. Krausbauer, E. F. Steigmeier, A. E. Widmer, H. F. Kappert, and G. Neugebauer, Growth and Physical Properties of LPCVD Polycrystalline Silicon Films, *J. Electrochem. Soc.*, Vol. 131, pp. 675–682, 1984.
90. R. Le Bihan, F. Karray, and B. Cambou, Grain Size and Resistivity of Polycrystalline Silicon Films, in: *Poly-Micro-Crystalline and Amourphous Semiconductors Symp.*, Strasbourg, France, 1984.
91. X. Zhang, T.-Y. Zhang, M. Wong, and Y. Zohar, Rapid Thermal Annealing of Polysilicon Thin Films, *J. Microelectromech. Sys.*, Vol. 7, pp. 356–364, 1998.
92. A. Pleschinger, J. Lutz, F. Kuchar, H. Noll, and M. Pippan, A Structural and Topographical Study of Low-Pressure Chemical-Vapor-Deposited Polysilicon by Scanning Probe Microscopy, *J. Appl. Phys.*, Vol. 81, pp. 6749–6753, 1997.
93. M. M. Mandurah, K. C. Saraswat, C. R. Helms, and T. I. Kamins, Dopant Segregation in Polycrystalline Silicon, *J. Appl. Phys.*, Vol. 51, pp. 5755–5763,

1980.

94. C. H. Henager, Jr. and W. T. Pawlewicz, Thermal Conductivity of Thin Sputtered Optical Films, *Appl. Opt*, Vol. 32, pp. 91–101, 1993.
95. J. E. Graebner, M. E. Reiss, and L. Seibles, Phonon Scattering in Chemical-Vapor-Deposited Diamond, *Phys. Rev. B*, Vol. 50, pp. 3702–3713, 1994.
96. E. Pop, K. Banerjee, P. Sverdrup, R. Dutton, and K. Goodson, Localized Heating Effects and Scaling of Sub-0.18 Micron CMOS Devices, in: *IEDM Tech. Digest*, pp. 31.1.1–31.1.4, 2001.
97. K. Fushinobu, A. Majumdar, and K. Hijikata, Heat Generation and Transport in Submicron Semiconductor Devices, *J. Heat Transfer*, Vol. 117, pp. 25–31, 1995.
98. S. Sinha and K. E. Goodson, Phonon Heat Conduction from Nanoscale Hotspots in Semiconductors, *Proc. 12th Int. Heat Transfer Conf.*, Grenoble, France, pp. 573–578, 2002.
99. G. Dolling, Lattice Vibrations in Crystals with the Diamond Structure, *Symp. on Inelastic Scattering of Neutrons in Solids and Liquids*, IAEA, Vienna, pp. 37–48, 1963.
100. C. H. Mastrangelo and R. S. Muller, Thermal Diffusivity of Heavily Doped Low Pressure Chemical Vapor Depositied Polycrystalline Silicon Films, *Sens. Mater.*, Vol. 3, pp. 133–142, 1988.